

Cooperative Lattice Dynamics and Anomalous Fluctuations of Microtubules

Hervé Mohrbach^{1,2}, Albert Johner² and Igor M. Kulić^{2*}

¹*Groupe BioPhysStat, Université Paul Verlaine-Metz, 57078 Metz, France and*

²*CNRS, Institut Charles Sadron, 23 rue du Loess BP 84047, 67034 Strasbourg, France*

(Dated: August 3, 2018)

Microtubules have been in biophysical focus for several decades. Yet the confusing and mutually contradicting results regarding their elasticity and fluctuations have shed some doubts on their present understanding. In this paper we expose the empirical evidence for the existence of discrete GDP-tubulin fluctuations between a curved and a straight configuration at room temperature as well as for conformational tubulin cooperativity. Guided by a number of experimental findings, we build the case for a novel microtubule model, with the principal result that microtubules can spontaneously form micron size cooperative helical states with unique elastic and dynamic features. The polymorphic dynamics of the microtubule lattice resulting from the tubulin bistability quantitatively explains several experimental puzzles including anomalous scaling of dynamic fluctuations of grafted microtubules, their apparent length-stiffness relation and their remarkably curved-helical appearance in general. We point out that tubulin dimers' multistability and its cooperative switching could participate in important cellular processes, and could in particular lead to efficient mechanochemical signalling along single microtubules.

PACS numbers: 87.16.Ka, 82.35.Pq, 87.15.-v

INTRODUCTION

Microtubules (MTs) are fascinating biological macromolecules that are essential for intracellular trafficking, cell division and maintaining the cell shape. They display unique elastic and dynamic behavior, inherited by their complex self-assembling nanotube structure. Surprisingly, despite an enormous accumulation of knowledge about their structure, the MTs static and dynamic properties have challenged all attempts of a fully coherent interpretation. In this paper we develop the line of thoughts leading towards a new theory that provides a more comprehensive understanding of these MT's properties. The fundamental result is that stabilized MTs spontaneously form large scale superhelices of micron size pitches and diameters. The MT's super-helical structure turns out to be a consequence of a cooperative interaction between its individual subunits that can sustain several stable curved conformations. Cooperativity of fluctuating internal degrees of freedom in combination with the cylindrical MT symmetry lead to a helical state with very unique characteristics in the world of macromolecules: MTs are helices that are permanently but coherently reshaping -i.e. changing their reference ground state configuration- by thermal fluctuations. In particular when clamped by one end MTs undergo an unexpected zero energy motion. As we will see, this could be the key for a consistent interpretation of certain challenging experimental results not captured by the conventional scenarios and models. It is worth remarking, that the large majority of experiments probing the above mentioned properties are in-vitro experiments on MTs with stabilizing drugs. We stress this point, as the experimentally prevalent presence of stabilizing agents is not innocent and could modify MT's properties. Neverthe-

less there are reasons to believe that the theory developed here might be valid also for non treated MTs.

Before embarking on the road to a "polymorphic MT theory", we first review the conventional understanding of the common MT properties as well as some key experiments which will be our necessary guides towards the model we propose. This paper which extends and deepens a previous short presentation of the idea of polymorphic MTs [1] is written in two parts. In the first part, we provide conceptual and graphical explanations of the ideas behind the model and investigate consequences of the here developed polymorphic MT model. We hope that this part is self consistent and didactic enough, so that a general reader can grasp the basic underlying ideas. In the second more technical part, the mathematical model is developed and quantitative results are presented. The details and derivations are left to an extensive appendix.

SHORT REVIEW OF WHAT WE UNDERSTAND ABOUT MICROTUBULES

Microtubules are cytoskeletal protein filaments of eukaryotic cells fulfilling different structural and mechanical functions in the cell: MTs act as "cellular bones" strongly influencing the cell shape, constitute the main routes for molecular motor mediated intracellular cargo transport [2, 3] and perform other important tasks like stirring the cytoplasm [4]. Besides, MTs play a central role in the assembly of the mitotic spindle during cell division and are at the heart of the functioning of cilia and flagella [5]. This versatility of MTs in a variety of biological functions mainly relies on their unique high stiffness and on their dynamics of assembly and disassembly.

The high rigidity of MTs (similar to hard plastic) is due to their structure that is known in exquisite detail from 3D electron microscopy reconstructions [6, 7]: MTs are hollow tubes whose walls are formed by assembly of a variable number N of parallel protofilaments (PFs). The PFs themselves are built by head-to-tail self association of the $\alpha\beta$ -tubulin heterodimer protein subunit (yielding a polarity to MTs) whose structure has been resolved by electron crystallography [8, 9].

In vivo, MTs most commonly appear with 13 PFs [10] (although there are exceptions depending of the cell type), whereas in vitro a variety of structures with PF number ranging from $N = 9$ to 16 were observed [11, 12]. Transitions of different lattice types (mostly with the gain or loss of one PF) within a single MT are also frequent [13–15]. The MT lattice can accommodate for these different structures by twisting the PFs around the central MT axis although this process is energetically costly. The typical lattice twist repeat lengths (pitches) are: $+3.4, +25, -6\mu m$ for $N = 12, 13$ and 14 PF MTs respectively, with $+/-$ denoting right/left-handed twist [11–15]. As we will see the lattice twist is an essential property of the model that we will propose later on. Any deviation from the most frequent, energetically favorable and thus less twisted configuration $N = 13$ implies an internal prestrain in the MT lattice. The latter stress can locally deform the end portions of the lattice or even destabilize it [16].

Another internal prestrain in the MT lattice is believed to be caused by the tubulin subunit which upon incorporation into the lattice hydrolyzes a bound GTP molecule converting it quickly into a GDP-tubulin form which has the tendency to form a curved state - curling radially away from the axis [17, 18]. The constraint imposed by the MT lattice however maintains the GDP-tubulin dimers in a straight unfavorable state - in turn trapping mechanical prestrain. In this conventional view MTs are seen as internally prestrained but intrinsically straight Euler beams. The GDP-tubulin prestrain is also believed to trigger rapid depolymerization called the polymerization "catastrophe" [19]. The stability of MT is regulated either by the presence of a thin layer of yet unhydrolyzed GTP tubulin dimers at the growing MT end (the so called GTP-cap-model, [20, 21]) or by the binding of MT-associated proteins (MAP) or of drugs such as taxol.

WHAT WE DON'T UNDERSTAND ABOUT MICROTUBULES

Mechanical properties of stabilized MTs

To investigate the mechanical properties of the MT lattice the presence of the polymerization dynamics is often an obstacle. As previously mentioned it can be switched

off by stabilizing agents like taxol or MAPs. In the bulk of the available in vitro studies taxol stabilization has been the experimental method of choice for investigating the elastic properties of MT. It is believed that taxol maintains tubulin dimers in an approximately straight conformation and thus prevents depolymerization [22–24]. However, direct EM investigations of single taxol-GDP-PFs [25] reveals a more complex and interesting picture. A taxol stabilized single PF can in fact coexist in several conformational states with comparable free energies: a straight state $\kappa_{PF}^{st} \approx 0$ and a weakly curved state with intrinsic curvature $\kappa_{PF}^{wc} \approx 1/250nm$ (see Fig. 1a). A third highly curved state with $\kappa_{PF}^{hc} \approx 1/20nm$ additionally appears after longer observation periods. Notably Elie-Caille et al. [25] pointed out a cooperative nature of the straight to curved transition within single PFs. These important findings - several conformational tubulin dimer states and cooperative interaction between them - will be one central ingredient of our model later on.

Going from a single protofilament to the whole tube, a central mechanical property of interest often measured for stabilized MTs, is its persistence length defined as $l_p = B/k_B T$. Here $B \propto Y$ stands for the flexural rigidity which is for an isotropic beam proportional to its elastic Young modulus Y . The persistence length is the length scale characterizing the filament's resistance to thermally induced bending moments. Several experimental approaches have been developed to measure bending stiffness of taxol stabilized MTs. One method consists in measuring MT's thermal shape fluctuations via dark-field microscopy [26, 27] or fluorescence light microscopy [28]. Alternatively in several other experiments, l_p has been determined by applying controlled bending forces via hydrodynamics [27], optical tweezers [29–32] and atomic force microscope tips [33]. Interestingly the authors in [26] observed that stabilized MTs are not perfectly straight, but contain some form of quenched curvature disorder which needs to be subtracted from the measurements. In the same vein, the observations from dark-field images of the thermal fluctuations of the free end of axoneme-bound MTs, show that taxol stabilized MTs adopt a three-dimensional helicoid structure [27] (we will return to this point later on).

The persistence length obtained from these different experiments is set in the range of 1 to 8 mm with some of newer studies going down to 0.1 mm (cf below). For a standard semiflexible polymer (like e.g. actin or DNA) we expect l_p to be a material constant, in particular independent of the filament's length. However, for MTs, the experimental l_p data are not only highly scattered but extremely confusing on this point. That the persistence length could indeed depend on the MT length was first mentioned and observed in references [31, 32] and confirmed by other experimental measurements - probing either the thermal movement [34] or the active bending deformations by electrical fields of individual taxol stabi-

lized MTs gliding on a kinesin-coated surface [35, 36]. In particular these techniques gave for short MT segments with submicron length a persistence length between 0.08 and 0.24 mm .

This intriguing "length dependent stiffness" was also investigated by Pampaloni et al who measured the lateral fluctuations of MTs grafted to a substrate [37]. These authors found a l_p falling within a range of 0.11 to 5.04 mm for MT lengths varying from 2.6 to 47.5 μm - with a strong linear length- l_p correlation. A similar experiment done in [38] measured the longest relaxation time $\tau_{max}(L)$ of MTs for various MT lengths L . It was found that MTs exhibit unusually slow thermal dynamics compatible with $\tau_{max} \propto L^3$ (cf. Fig 9) - in sharp contrast to standard semiflexible filaments with $\tau_{max} \propto L^4$. In [39], the relaxation time for long MTs ($L > 10\mu m$) extracted from a 2-D shape analysis of taxol stabilized fluorescent MTs shows an anomalous dynamics on short scales as well. Furthermore it has also been experimentally found that the rigidity of MTs depends on their growth velocity [40]. All these experiments measuring the bending stiffness and the bending dynamics brought the community to the conclusion that the "beam of Life" cannot be seen as a simple Euler beam. Its complex internal structure should determine its elastic and dynamical properties. But which internal mode contributes to the now obvious elastic complexity, is the important question - a convincing answer of which is still missing.

Helices and Rings

Even more intriguing than the issue of MT elasticity is perhaps the question : What is the ground state of a MT? While the naive answer - a straight rod - would be the most accepted view, a number of experiments put this mundane simplistic picture in doubt. For instance, wavy sinusoidal and circular shapes are frequently observed when MTs are adsorbed to glass surfaces or confined between them. In this confined case the Fourier mode analysis of MT deformations systematically reveals that a few discrete modes have a larger amplitude than the fluctuations around them [26, 39, 40], cf. also [41]-supplementary material. This is a strong hint towards the presence of some type of "frozen in" curvature - dynamically quenched on experimental timescales. Likewise in motility assays, it is often seen that when MTs glide over a surface coated with molecular motors they follow wavy sinusoidal and often circular tracks [42, 43], cf. Figs. 1b. In this context, particularly interesting is the observation by Amos & Amos [42] of the formation of permanently circling MTs (see Figs 1b). These unusual stable circular gliding structures persisted for many cycles and occasionally straightened again. As written by the authors [42], this suggests that "an intact tubular polymer is capable of holding more than one conforma-

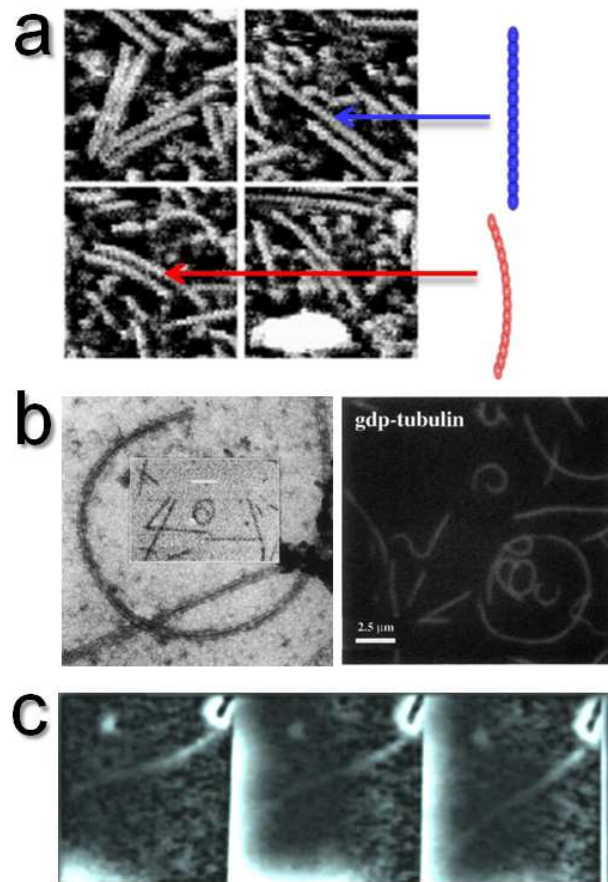


FIG. 1: The empirical evidence for tubulin bistability: (a) A single taxol stabilized protofilament can coexist in a straight $\kappa_{PF} \approx 0$ and a slightly curved $\kappa_{PF} \approx 1/250nm$ state (reproduction from [25]) (b) Taxol stabilized microtubules in gliding assay experiments can switch to a stable circular state and move on circular tracks (from [42][43]). Microtubules are occasionally observed to switch back and forth between the circular and straight states. (c) Taxol stabilized microtubules form a three-dimensional helicoid structure with a $15\mu m$ pitch (from [27]).

tional state without the help of an external force". From EM images it was inferred that the underlying mechanism stems from the balance of individual taxol-GDP-tubulin dimers between two or more different stable conformations [44].

An even more clear hint towards the real nature of the "frozen in" curvature was -as already mentioned- discovered by Venier et al [27] (Fig.1c) who described stabilized MTs as *wavy periodic shapes* with a half period of about $7 - 8\mu m$. This observation combined with the fact that MTs often went out of focus, lead the authors to "suggest that taxol-treated microtubules may adopt a three-dimensional helicoid structure of $15\mu m$ pitch".

Therefore it seems that the MT curvature is a persis-

tent attribute attached to its lattice. Any serious attempt to fully understand the complexity of MT elasticity can not avoid the question of its ground state. Indeed understanding fluctuations around a particular state will be futile as long as the origin of the state itself remains in the dark.

The Soft Shear Model

A first theoretical attempt to cope with some aspects of the described MT mechanical complexity was the "soft shear model" (also called "Timoshenko beam model", or "anisotropic composite material model") [33, 37, 45, 46]. In this model the MT is considered as an anisotropic fiber-reinforced material [33, 37] with the tubulin protofilaments acting as strong fibers weakly linked with easily shearable inter-protofilament bonds. Some specific equilibrium statistical and mechanical properties of that model were investigated in [45, 46]. An interesting peculiarity and inherent consequence of this model is that any local lattice deformation gives rise to a long distance curvature relaxation [46] and can lead to a long range interaction along the MT contour. This aspect of the "soft shear model" (SSM) is in phenomenological agreement with cooperative deformations induced by enzymes like katanin. Furthermore this model predicts a length-dependent persistence length which approximately resembles the measured behavior [37, 38]. However in detail it suffers a number of difficulties and inconsistencies in particular :

- The ground state of SSM is straight - in conflict with the helical ground state observation [27].

- The SSM does not allow for lattice multistability as observed by Amos& Amos [42].

- The predicted value of the shear modulus is extremely small [37, 38, 46] ($10^5 - 10^6$ times smaller than the Young modulus). This would imply very strong shearing in bent microtubule structures. This however is unsupported by other experimental evidence. Indeed observations of straight and highly bent MTs shows that bending does not significantly modify the relative position of the inter-protofilament bonds [47].

- The dynamics of clamped MTs [37, 38] does not come naturally out from the SSM. To reach agreement and fit the experimental dynamics the shear model needs to introduce an ad hoc internal dissipation of unclear origin.

- For short MTs ($< 4\mu m$) that model is very far off and disagrees with the "plateau" region of the bending stiffness vs length relations (cf. Fig 3 in [38]).

A careful reanalysis of clamped MT experiments, cf. Figs. 2,3 in [37, 38], reveals two features not captured by the SSM : the persistence length scales for large L approximately as $\sim L$ (without signs of saturation) while the relaxation times scale as $\sim L^3$. This exotic behavior naively suggests the presence of a limited angu-

lar hinge at the MT clamping point. On the other hand artifacts that could trivially lead to a "hinged behavior" (like loose MT attachment and punctual MT damage) were specifically excluded in experiments [37, 38].

Facing all these obstacles it becomes increasingly clear that the solution to all puzzles requires a cut and a radically different hypothesis.

IDEA OF POLYMORPHIC MICROTUBULE DYNAMICS

The new scenario proposed here is based on the hypothesis of *cooperative internal* MT lattice dynamics. The two central assumptions of our model are as follows:

- (I) The taxol-GDP-tubulin dimer is a conformationally multistable entity and fluctuates between at least 2 states on experimental time scales : a straight and an outwards curved state (Figs. 1a and 2a).

- (II) There is a nearest-neighbor cooperative interaction of tubulin states along the PF axis.

Note that assumption I is very different from the conventional picture where GDP-tubulin has only *one* energetically favorable (curved) state. We will show that a model based on I and II straightforwardly leads us to the very origin of MT (super) helicity and provides a coherent explanation for static and dynamic measurements in thermal fluctuation experiments.

In contrast to the soft shear model, the present model is elastically isotropic but the monomer curvature is bistable. As we will see, the ground state in this new model is a highly degenerate 3 dimensional helix fluctuating between many equivalent configurations.

Conformational Symmetry Breaking and Helix Formation

In this chapter we will give a simple pictorial panorama over the consequences of assumptions I and II. What happens when tubulin dimers obeying assumption I are trapped in the circularly symmetric MT lattice? Starting from assumption I we imagine that the straight and curved GDP-tubulin state have a certain energy difference $\Delta G > 0$, with the curved state being slightly more favorable. The strict preference for the curved state is however only true if the tubulin dimers are free i.e. not confined to the lattice. The situation becomes more interesting once they are incorporated into the lattice. Obviously the outwards bending tendency of the curved state is in conflict with the geometry of the lattice. Switching a dimer on one MT side will frustrate the dimers on the opposite side of the tube and prevent them from switching at the same time. On the other hand the direct neighbors of the curved dimer (on the same MT side) will profit and switch easier to the curved state, as the lattice is already

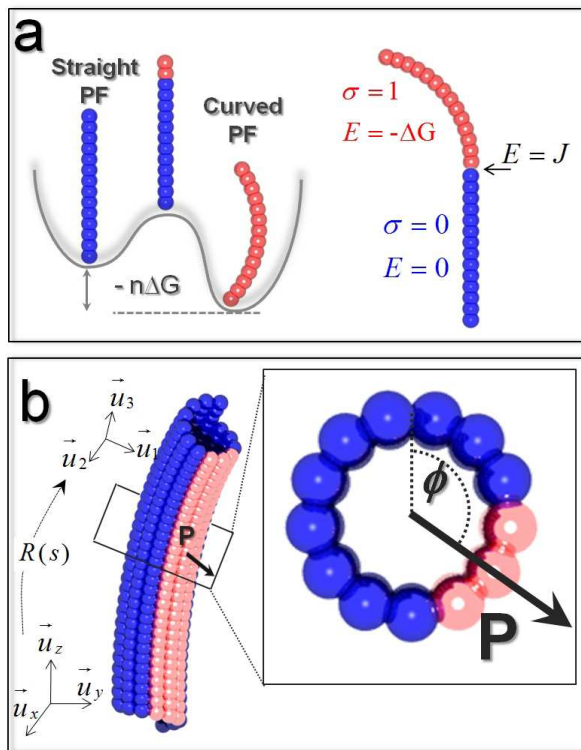


FIG. 2: Elements of the "polymorphic tube model". (a) The GDP-tubulin protofilaments can fluctuate cooperatively between two discrete states. The curved $\sigma = 1$ state is energetically preferred over the straight state $\sigma = 0$ with an energy gain $E = -\Delta G$. The junction between straight and curved states along the same protofilament are penalized by a coupling constant $E = +J$. b) Competition between tubulin switching energy and elastic lattice strain energy leads to spontaneous symmetry breaking: MT bends to a randomly chosen direction and assumes a non-zero polymorphic order parameter P . The energy becomes invariant with respect to an arbitrary rotation of the polymorphic phase angle ϕ .

slightly "pre-bent" in the correct direction. This peculiar interplay of negative and positive interaction gives rise to a clustering of curved dimer states into a single block on one side of the tube cf. Fig. 2b.

This immediately raises the question about the orientation of this curved dimer block. Which MT side will be selected, and in which direction will the MT overall bend, can only be decided by the process of *spontaneous symmetry breaking*. That is, if the ground state is a curved dimer block, it will be a highly degenerate state (see Fig. 3). In turn it can be expected to thermally move through the lattice at next to no energy cost (apart from some friction)! This is the most essential feature of the present model.

So far we have considered only a single MT cross-section. If the assumption II (cooperativity) would not hold the curved state blocks would pick their sides at each section completely independently. The tube would

locally curve in random uncorrelated directions and the effect of tubulin multistability would stay essentially invisible on the larger scale. However according to assumption II the blocks become correlated in orientation and prefer to stack on the top of each other. This then leads to macroscopically a bent - in fact a circular MT - if the PF were not twisted around the central MT axis (see Fig. 2b). This provision brings us to the last interesting point. As already mentioned MT lattices are generically twisted i.e. their PFs are not strictly parallel. With a cooperative interaction along the PFs - which are now twisting around the tube axis - the final product of assumption I and II will be a long pitched helix! The pitch of the helix should coincide with the lattice twist repeat length: $+3.4, +25, -6\mu m$ for $N = 12, 13$ and 14 PF MTs respectively. The created "polymorphic helix", however will not be unique and will be able to reshape between its N indistinguishable orientation states.

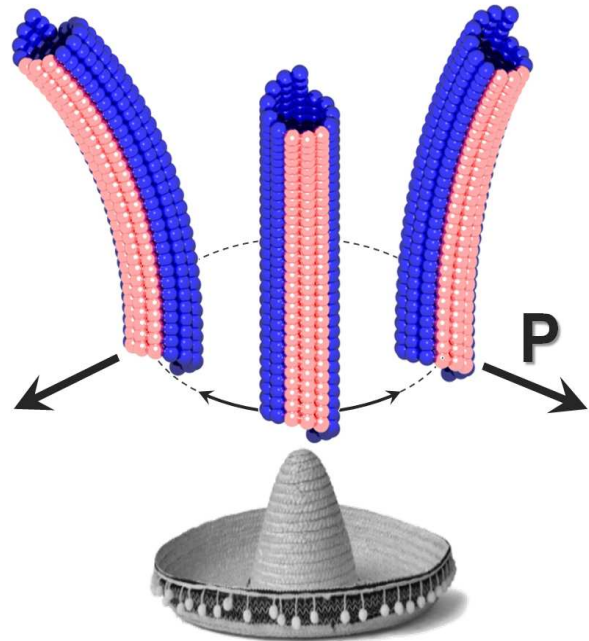


FIG. 3: The straight state of the microtubule becomes unstable and forms a spontaneous bend with fixed curvature pointing towards a randomly chosen direction. The microtubule can assume one of the N degenerate ground states and switches between them at no energy cost - the effective potential has a shape reminiscent of a Mexican hat.

When we graft one end of such a polymorphic helix onto a surface (as e.g. performed in [37, 38]) the helix will still be able to switch between the equivalent orientations and perform a motion that we call "wobbling" (see Fig. 4). It is exactly this type of motion that can give rise to the static and dynamic effects measured in [37, 38].

To see this we can approximate the movement of a

clamped polymorphic helix that is switching between its equivalent ground states with a "rigid conical rotor" (see Fig. 4). For such a rotor the transverse displacement ρ of the MT end grows linearly with its length L . Using the naive definition of persistence length $l_p \approx L^3/3 \langle \rho^2 \rangle$ (where $\langle \rangle$ is the ensemble average) and the fact that $\langle \rho^2 \rangle \propto L^2$ this apparent persistence length becomes proportional to the length $l_p \propto L$. This scaling (cf. Fig. 11) is in agreement with the experimental results in [37, 38] giving us the first hint that the model is on the right track. Appendix E comments on the robustness of this conical hinge-like motion against a limited local hindrance of the wobbling mode due to the adsorbed part of the grafted MT.

A further encouragement comes from the study of the dynamics of the model. Making again the approximation of a rigid conical rotation (induced by wobbling) the observed unusual scaling of the longest relaxation time $\tau_{\max} \propto L^3$ can also be easily understood. In fact a slender object of length L rotated along a conical surface has a friction constant $\xi_{rot} \propto L^3$. In turn the longest relaxation time is given by diffusional equilibration time on the cone, i.e. $\tau_{\max} \propto \xi_{rot}/k_B T \propto L^3$ (cf. Fig. 12). It turns out that the model correctly predicts both the exponent and the prefactor of the experimental relaxation time.

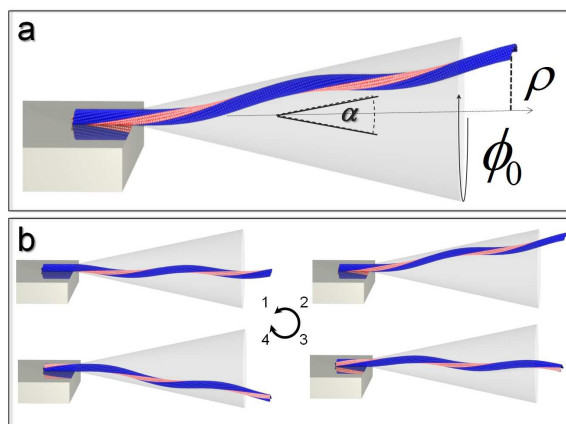


FIG. 4: Clamped polymorphic microtubule with intrinsic lattice twist attached at its end to a substrate [37][38] performs a peculiar movement. It forms a polymorphic helix with N degenerate ground states and switches between them at no energy cost. The approximately conical motion with opening angle α leads to anomalous lateral fluctuations $\langle \rho^2 \rangle \sim \alpha^2 L^2$ - radically different from all other semiflexible filaments.

In addition it is further reassuring that the helical ground state(s) of the model provides a rationale for the observation of MT helices by Venier et al. [27].

In Vivo Implications of Microtubule Polymorphism

The bulk of observations cited here is made in vitro on taxol stabilized MTs. It is known that taxol inhibits MT disassembly by maintaining the tubulin dimer in a state that strongly favors polymerization. But from the experiments reported above it is also clear that taxol does not suppress all tubulin conformational changes : taxol-GDP-tubulin dimer has multiple stable conformations [25]. How do these in vitro findings relate to MTs in vivo?

It is a common empirical observation in many in vivo systems that despite their high bending stiffness MTs are often seen curved or highly wavy on micron scales [39, 48–52]. For instance in [48], highly sinusoidal MTs on the periphery of living LLC-PK1 cells were observed. These shapes are usually explained as a consequence of motor induced buckling opposed by a gel-like environment that leads to finite wavelength- buckling [49]. While the "buckling in a gel" interpretation is physically appealing a closer look at the data in [49] (in particular the accompanying movie material) reveals an absence of correlation in buckling *directions* of neighboring MTs. This observation puts a question mark on the participation of a background continuum gel - as in this case the strains in the gel would necessarily propagate to neighboring microtubules and lead to spatially correlated buckling events - in sharp contrast with observations. Therefore we are left with a robust phenomenon of sinusoid, constant wavelength MTs - however without a definite interpretation so far.

The phenomenology of stable rings [42] and wavy sinusoid MTs forming in gliding assays [43] is strikingly similar and visually indistinguishable from the pure in vivo observations [39, 48–52]. Indeed, in both situations highly curved lattice states of very similar magnitudes $\kappa_{MT} \approx 1 - 2 \mu m^{-1}$ are readily observed. This analogy between in vivo and vitro cases suggests that tubulin dimers - both in vivo and taxol stabilized (in vitro) possess an identical highly curved state ($\kappa_{PF}^{h.c.} \approx 1/20nm$). This highly curved state appears to be activated within the lattice only under compressive loads and seems to be a universal property of GDP tubulin itself - independent of taxol stabilization.

On the other hand the weakly curved state of taxol-GDP-dimer ($\kappa_{PF}^{w.c.} \approx 1/300nm$) is soft enough to be activated by thermal fluctuations. The empirical evidence for the weakly curved state in vivo is far less obvious than for the highly curved state. The slight deformations induced by the former would be more difficult to distinguish from other MT deforming effects in living cells like motors, polymerization forces, presence of lattice defects, bundling and microtubule associated protein action. However the observed phenomenology of length dependent persistence length of MTs growing from cen-

trosomes in egg extracts [53] (no taxol present) resembles qualitatively and quantitatively the in vitro observations [37, 38]. This is one more indication that the dynamic MT polymorphism could persist also in vivo.

At least two possible biological implications of the helicoidal polymorphic MT nature come straight to mind. First, a curved or helical beam under compressive load responds like a mechanical spring and is therefore much softer (in tension, compression and bending) than a straight beam. Therefore a network of helical MTs might be important for the overall mechanical compliance of the cell. A perfectly straight MT buckled by an extracellular load would be much more susceptible to mechanical failure and depolymerization than a soft compliant helix. Second, helical shapes are geometrically (topologically) prevented from side-by-side aggregation, can thus evade the formation of bundles and instead form loose networks with much fewer contacts. It appears that a tuned helicity (that can be switched on or off) could be a good mechanical control parameter for the formation of different cytoskeletal structures. While the bulk of the cytoplasmic MTs is preferably in the loose network state (favored by helicity) in occasional situations like the neuronal axons straight aligned MTs are required. In such a situation the bundling could be triggered by switching the lattice to the straight state. Remarkably in the process of axonal retraction the straight axonal bundle is destabilized (and eventually contracted towards the cell soma) by an apparent transition of the MTs to a wavy coiled state [54] very reminiscent in shape to single wavy MTs from cell soma [39, 48–52].

In general MT's polymorphism might have other, less obvious biological implications that still have to be identified. In particular a more speculative possibility is that the tubulin's allosteric multistability might also be a piece in the puzzle of MT "catastrophes". A cooperative curvature switch might trigger a transition from growth to depolymerization. Maybe the most fascinating aspect could lie in the possibility of signal transmission along single MTs via a long range conformational switch. If our model is correct this is the most inherent and distinct consequence of the underlying mechanism.

We conclude here the qualitative description of essential ideas behind the polymorphic tube model. In the following we switch gears and present in more quantitative detail the mathematical model. The mathematically less inclined reader is invited to fly over some figures, comparisons with experiments, maybe pick up additional concepts (such as polymorphic defects and their dynamics) and jump to the perspectives section which will underline the essential biological consequences.

THE POLYMORPHIC TUBE MODEL

Until now the discussion was qualitative and in the following we build the mathematical model of the polymorphic MT. We will provide quantitative arguments and model experimental data, justifying thus a posteriori the previous discussion. In this section, we will focus on the thermally induced weakly curved state in taxol-stabilized MTs and leave the case of mechanically induced highly curved MTs for further works.

We model the GDP-tubulin dimer state by a two state variable $\sigma_n(s) = 0, 1$ which corresponds to the straight and curved state at each lattice site. The $n = 1, \dots, N$ is the circumferential PF index and $s \in [0, L]$ is the longitudinal position variable along the MT centerline. We recall that our model is based on the following assumptions:

(I) The taxol-GDP-tubulin dimer fluctuates between 2 states - straight and curved - (Fig. 2a) with an energy difference $\Delta G > 0$ favoring the curved state. The energy density resulting from the switching of tubulin dimers (at a given MT section) is then given by

$$e_{trans}(s) = -\frac{\Delta G}{b} \sum_{n=1}^N \sigma_n(s) \quad (1)$$

with $b \approx 8nm$ the dimer length.

(II) There is an Ising type nearest-neighbor cooperative interaction of tubulin states *along* the PF axis with an interaction energy $J > 0$ favoring nearest neighbor dimers on the same PF to be in the same state. This leads to the interaction energy density:

$$e_{inter}(s) = -\frac{J}{b} \sum_{n=1}^N (2\sigma_n(s) - 1)(2\sigma_n(s+b) - 1) \quad (2)$$

The last term missing in our description is the elastic energy density of the MT lattice. For a usual isotropic Euler beam the material deformations ε are related to the centerline curvature vector $\vec{\kappa}$ via $\varepsilon = -\vec{\kappa} \cdot \vec{r}$ with \vec{r} the radial material vector in the cross-section. For a polymorphic MT, modelled as a continuum material made of N PFs ($N = 11 - 16$), its actual deformation will depend on the polymorphism-induced prestrain ε_{pol} . In this case the elastic energy density of the MT can be written as

$$e_{el}(s) = \frac{Y}{2} \int_{R_i}^{R_o} \int_0^{2\pi} (\varepsilon - \varepsilon_{pol})^2 r dr d\alpha \quad (3)$$

where the integration in e_{el} goes over the annular MT cross-section with $R_i \approx 7.5nm$, $R_o \approx 11.5nm$ the inner and outer MT radii respectively. The prestrain ε_{pol} is a function of the polymorphic state of the tubulin dimers. Its definition requires a decomposition of the tubulin dimer in an inner part (facing the tube axis) and an outer part (facing from the tube axis outwards), cf. Fig 5. We assume that each curved

dimer state generates a positive prestrain $+\varepsilon_{PF}$ on its inner part and an equal but negative prestrain $-\varepsilon_{PF}$ on its outer part. We can then write $\varepsilon_{pol}(s, r, \alpha) = \varepsilon_{PF} \sigma_n(s) [I_{[R_i, R_o - d_{PF}/2]}(r) - I_{[R_o - d_{PF}/2, R_o]}(r)] \cdot I_{[\frac{2\pi}{N}n + q_0s, \frac{2\pi}{N}(n+1) + q_0s]}(\alpha)$ where $I_{[\cdot]}(x) = 1$ if $x \in [\cdot]$ and 0 otherwise (Heaviside function) and d_{PF} is the PF diameter. The parameter q_0 appearing in the angular part of ε_{pol} is the natural lattice twist that leads to the proper geometric rotation of a PF around the tube axis. This parameter is lattice type dependent and takes discrete values $2\pi/q_0 = +3.4\mu m, +25\mu m, -6\mu m$ for $N = 12, 13$ and 14 PF MTs respectively [11, 12][13][15]. We can estimate the prestrain ε_{PF} from the experimental value of the single switched PF's curvature $\kappa_{PF} \approx (250nm)^{-1}$ -measured in Ref.[25] on single taxol-stabilized PFs - to be $\varepsilon_{PF} = d_{PF}\kappa_{PF}/2 \approx 10^{-2}$. Collecting all energy contributions together the total elastic + polymorphic energy of the MT is then given by

$$E_{MT} = \int_0^L (e_{el} + e_{trans} + e_{inter}) ds. \quad (4)$$

The ground state within this model is determined by the interplay of the first two terms e_{el} and e_{trans} . The last term e_{inter} rules over cooperativity and is responsible for the suppression of defects in the ideal polymorphic order (cf. Fig. 7). A large value of the cooperativity constant with $J \gg k_bTL/b$ would imply a defect free lattice. However the presence of the latter defects (and their motion) are a necessary ingredient for the overall rearrangement of the helix as discussed later on.

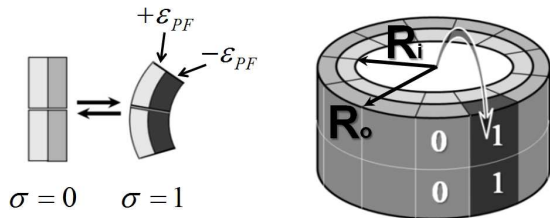


FIG. 5: Strains and deformations in the polymorphic tube model. Each tubulin dimer can fluctuate between a straight state $\sigma = 0$ and a curved state $\sigma = 1$ of intrinsic curvature κ_{PF} . The curved tubulin dimer generates a positive prestrain $+\varepsilon_{PF}$ on its inner part and an equal but negative prestrain $-\varepsilon_{PF}$ on its outer part with strains related to observed dimer curvature via $\varepsilon_{PF} = (R_o - R_i)\kappa_{PF}/2$.

To understand the basic behavior of the ideal helical ground state without defects - i.e. PFs are individually in a uniform state (either curved or straight)- we initially restrict ourselves to the simplified energy density $e = e_{el} + e_{trans}$. To investigate the MT geometry we first introduce two reference frames (Fig. 2b). One is the material frame with base vectors $(\vec{u}_1, \vec{u}_2, \vec{u}_3)$ attached to

the MT cross-section. The other is an external fixed laboratory frame with base vectors $(\vec{u}_x, \vec{u}_y, \vec{u}_z)$. Putting the MT along the \vec{u}_z axis direction and considering small MT angular deflections we have $\vec{u}_z \approx \vec{u}_3$. In this case the two frames are simply related to each other by a rotation transformation $R(s)$ given by the internal MT lattice twist q_0 , such that $(\vec{u}_x, \vec{u}_y) = R(s)(\vec{u}_1, \vec{u}_2)$ with

$$R(s) = \begin{pmatrix} \cos q_0s & -\sin q_0s \\ \sin q_0s & \cos q_0s \end{pmatrix} \quad (5)$$

To rewrite e in a more illuminating fashion, we define two important order parameters at each MT cross-section. The first one of them is the *vectorial polymorphic order parameter*

$$\vec{P}(s) = \sum_{n=1}^N \left(\vec{u}_1 \cos \frac{2\pi n}{N} + \vec{u}_2 \sin \frac{2\pi n}{N} \right) \sigma_n(s)$$

Physically, \vec{P} - a 2D vector at each local material frame section attached to the MT (cf Fig. 2b)- describes the asymmetry of distribution - a kind of "polarization" - of the dimer states. It acquires a non zero value only in the case when the curved and non-curved states are azimuthally separated on opposite MT sides. For instance the "all-straight" or "all-curved" PF state correspond both to the same value $\vec{P} = 0$. Besides the vector \vec{P} we need to define a second (scalar) quantity

$$M(s) = \sum_{n=1}^N \sigma_n(s)$$

which counts the total number of dimers in the curved state at cross-section s - or in the Ising model terminology : the "magnetization". After integration of Eq. 3 over the cross-section and some algebra the energy density $e = e_{el} + e_{trans}$ can be written in a more appealing form:

$$e = \frac{B}{2} \left[(\bar{\kappa} - \bar{\kappa}_{pol})^2 + \kappa_1^2 \left(\frac{\pi}{N} \gamma M - \sin^2(\pi/N) \vec{P}^2 \right) \right] \quad (6)$$

with the elastic bending modulus $B = \frac{Y\pi}{4} (R_o^4 - R_i^4)$, with $\kappa_1 = \frac{(R_o - R_i)^2}{\pi(R_o^2 + R_i^2)} \kappa_{PF}$ and a dimensionless parameter

$$\gamma = \frac{\kappa_{PF}}{\kappa_1} - \frac{2N\Delta G}{bB\kappa_1^2} \quad (7)$$

For small deviations of the tube axis from the \vec{u}_z direction, the polymorphic curvature vector $\vec{\kappa}_{pol}$ in the external coordinate frame (\vec{u}_x, \vec{u}_y) is related to \vec{P} (in the internal frame (\vec{u}_1, \vec{u}_2)) via the transformation in Eq. 5:

$$\vec{\kappa}_{pol} = cR(s)\vec{P} \quad (8)$$

with $c = \sin(\pi/N) \kappa_1$ a geometric proportionality constant.

Phase Diagram

In the absence of defects the energy expression Eq. 6 allows us to determine the conformational ground state of a polymorphic MT. To this end, we first resort to one further small simplification and make the "single block ansatz", i.e. at each cross-section we assume only a single continuous block of p switched PFs. This ansatz was previously used by Calladine and has been proven very useful in modelling bacterial flagellin polymorphic states [55, 56]. In the ground-state configuration the curvature is given by $\vec{\kappa} = \vec{\kappa}_{pol}(p)$ whose absolute value obtained from Eq. 8 is $\kappa_{pol}(p) = \kappa_1 \sin(\pi p/N)$. The optimal switched block size $p = p^*$ can be determined by minimizing the second term in Eq. 6 which within this ansatz becomes

$$e = \frac{B\kappa_1^2}{2} \left(\gamma \frac{\pi}{N} p - \sin^2 \left(\frac{\pi}{N} p \right) \right) \quad (9)$$

This gives rise to an interesting MT phase behavior (cf. Fig. 6). The latter only depends on the polymorphic-elastic competition parameter γ from Eq. 7 -that measures the ratio between polymorphic energy of tubulin switching and the purely elastic cost of this transition.

For $\gamma < -1$ the chemical switching potential ΔG strongly dominates the elastic energy cost $bB\kappa_1^2$. Therefore switching is highly favorable and all the PFs will be found in the state $\sigma = 1$. This gives rise to a straight but highly prestrained configuration.

Analogously for $\gamma > 1$ the bending energy contribution is too costly for PFs to switch at all. Therefore in this regime the PFs are all in the straight state with $\sigma = 0$ and the MT is consequently straight as well.

For $-1 < \gamma < 1$ the situation is more interesting. In this interval we have a coexistence of two locally (meta) stable MT conformations: the straight tube (prestressed or not - depending on the sign of γ) and a curved lattice state with p^* switched protofilaments. For $-\bar{\gamma} < \gamma < \bar{\gamma}$ with $\bar{\gamma} \approx 0.72$ the curved lattice state is the absolute energy minimum and the straight state is only metastable. Therefore in this regime and in the absence of twist ($q_0 = 0$) the ground state configuration of the whole tube would be a simple circular arc section (cf. Fig. 2b). On the other hand, the ground state of a microtubule bearing natural lattice twist $q_0 \neq 0$ will be helical (cf. Fig. 4).

It is easy to see that a stable helical state as observed in [27] is only possible for a switching ratio $p^*/N \in [1/4, 3/4]$. This together with $\kappa_{PF} = 1/250nm$ from [25] and $\kappa_{pol}(p^*) = \kappa_1 |\sin(\pi p^*/N)|$ provides us with a direct estimate of the radius of curvature $\kappa_{pol}^{-1} \approx 9-14\mu m$. Very strikingly the latter range reproduces closely the observed MT helical curvatures as estimated from Venier et al. work [27] $\kappa_{measured}^{-1} \approx 11\mu m$ - lending strong support to the model. Furthermore, taking the helical state stability

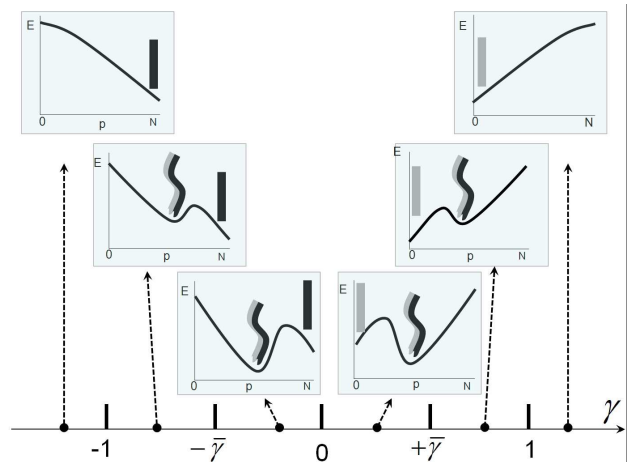


FIG. 6: The phase diagram of the polymorphic microtubule model as function of the polymorphic-elastic interaction parameter γ from Eq. 7. Depending of the magnitude and sign of γ the microtubule can be either in an "all PF switched state" (black), "no PF switched state" (grey) or in a mixed curved-helical state. Only the latter "mixed state" will display net curvature and lead to an observable helical appearance.

as an empirical fact (implying that $|\gamma| < 0.72$) and assuming a typical protein Young modulus $Y \approx 1-10GPa$, allows us a simple estimate of the transition energy per monomer $\Delta G \approx +1.1$ to $+11kT$ - a reasonable range for a soft biological object.

In general, the full energy expression -including the cooperativity energy term- Eq. 4 gives rise to a very complex behavior. Here we will focus on some basic new phenomena. It turns out that the most remarkable deviation from standard wormlike chain (WLC) behavior arises from the fluctuation dynamics of the polymorphic order parameter's angular phase that we consider in the following.

Polymorphic phase fluctuations

Here we introduce a slightly different phenomenological model that simplifies the study of Eq. 4 while still reflecting important aspects and physical properties of it. In this section we assume as before that the helical state is the ground state and consider now the effect of the fluctuations around it. To this end we decompose the polymorphic order parameter

$$\vec{P}(s) = P(s) [\cos(\phi(s)) \vec{u}_1 + \sin(\phi(s)) \vec{u}_2]$$

with $P(s)$ being the "polymorphic amplitude" and $\phi(s)$ the "polymorphic phase variable". The latter one determines the orientation of the switched block tubulin dimers at each cross section with respect to the MT material frame. From Eq. 8, the centerline curvature with

respect to a fixed external (\vec{u}_x, \vec{u}_y) frame is then:

$$\vec{\kappa}_{pol}(s) = \kappa_0 [\cos(q_0 s + \phi(s)) \vec{u}_x + \sin(q_0 s + \phi(s)) \vec{u}_y] \quad (10)$$

with $\kappa_0 = cP(s)$.

In general both the polymorphic phase ϕ and amplitude P can fluctuate along the MT contour and give contributions to the polymorphic energy. The phase fluctuations are induced by creation and motion of polymorphic "double defects", cf. Fig. 7. The double defect - a kind of "polymorphic dislocation" - that can be either left or right handed - maintains the number of switched protofilaments constant while reorienting the direction of curvature. At zero temperature the lattice would be defect-free, ϕ would be constant and the polymorphic order parameter \vec{P} would strictly follow the lattice twist. The phase change $\phi' \equiv d\phi/ds$ will deviate from zero if on relevant length scales there are enough polymorphic double defects to allow for a reorientation of the polymorphic order parameter away from optimum. The double defects carry only a limited local energy cost $\Delta E = 2J$ per defect and can be easily thermally excited if $J \lesssim k_B T$. In the approximation of a large number of PFs, assuming that ϕ can change continuously we can write the phase contribution to the energy as

$$E_{pol}(\phi) = \frac{C_\phi}{2} \int_0^L ds \phi'^2 \quad (11)$$

with the polymorphic phase stiffness $C_\phi \approx k_B T \frac{N^2 b}{8\pi^2} (2 + e^{2J/k_B T})$ which can be related to the density of double defects with energy $2J$ (cf. Fig. 7 and Appendix A), giving rise to a new length scale - the *polymorphic phase coherence length* $l_\phi = C_\phi/k_B T$. For MTs shorter than l_ϕ we will observe coherent helices while on longer length scales the helix softens significantly and loses eventually its helical appearance.

In contrast to the just discussed polymorphic dislocations which can be easily thermally excited, the variation of the polymorphic amplitude P , i.e., change of the number of switched PFs is more energetically costly. Any deviation of P from its optimum state P^* (given by the phase diagram) is associated with an energy cost $E \propto (|P| - |P^*|)^2 \cdot l$ proportional to the length l of the region in the unfavorable state, cf. Fig. 7 (see Appendix B). Therefore we conclude that on large enough scales the polymorphic phase fluctuations will be the dominant effect. Based on this and on the observation of stable helical states [27] we will in the following assume $P = const$.

For small deflections around the z -axis, the unit vector tangent to the MT's centerline is approximately given by $\vec{t} \approx (\theta_x, \theta_y, 1)$ in the laboratory frame $(\vec{u}_x, \vec{u}_y, \vec{u}_z)$ where $\vec{\theta} = (\theta_x, \theta_y)$ are the centerline deflection angles in x/y direction. The global centerline curvature $\vec{\kappa} = d\vec{t}/ds$ can then be approximated as $\vec{\kappa} \approx (\theta'_x, \theta'_y, 0)$ and the

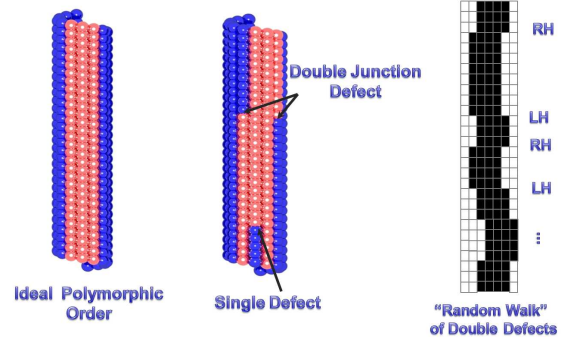


FIG. 7: Defects in ideal polymorphic order soften the helical states and give rise to "polymorphic dynamics". Single defects carry a cost proportional to their length, double defects only a local energy contribution. The coexistence of left- and right handed defects (LH and RH) along the length leads to a "random walk" of the polymorphic curvature direction and in turn to an effective torsional deformation.

total MT energy can be written as follows:

$$E_{tot} = E_{pol}(\phi) + E_{el}(\theta, \phi). \quad (12)$$

The first energy term is the polymorphic phase contribution Eq. 11. The second term is the elastic bending energy

$$E_{el}(\theta, \phi) = \frac{B}{2} \int_0^L (\vec{\theta}' - \vec{\kappa}_{pol})^2 ds. \quad (13)$$

From Eqs. 11-13, we see that the zero-temperature ground state corresponds to $\phi = const$ and $\vec{\theta}' = \vec{\kappa}_{pol}$ - that is to a defect-free helix with a pitch given by the natural lattice twist q_0 . At finite temperature, both elastic and polymorphic fluctuations will be excited so that the curvature can be decomposed as $\vec{\theta}' = \vec{\kappa}_{pol} + \vec{\theta}'_{el}$ with $\vec{\theta}'_{el}$ the purely elastic contribution. This gives rise to a helical MT shape described by the curvature $\vec{\kappa}_{pol} + \vec{\theta}'_{el}$ and torsion $\tau \sim \phi' + q_0$. The MT lateral displacements away from the z axis can be written as $\vec{\rho}(s) = (x(s), y(s)) = \int_0^s (\theta_x(s'), \theta_y(s')) ds'$ that for small deflections decouples into elastic and polymorphic displacements $\vec{\rho}(s) = \vec{\rho}_{pol} + \vec{\rho}_{el}$, where $\vec{\rho}_{el} \approx \int_0^s \vec{\theta}'_{el}(s') ds'$ and $\vec{\rho}_{pol} \approx \int_0^s \vec{\theta}'_{pol}(s') ds'$. The latter can also be written from Eq. 10 as

$$\vec{\rho}_{pol}(s) = \kappa_0 \int_0^s ds' \int_0^{s'} d\tilde{s} (\cos(q_0 \tilde{s} + \phi(\tilde{s})) \vec{e}_x + \sin(q_0 \tilde{s} + \phi(\tilde{s})) \vec{e}_y) \quad (14)$$

In Fig. 8, snapshots of configurations of clamped MT obtained from Monte Carlo simulations are plotted for different concentrations of double defects (i.e. different values of l_ϕ) with twist and no twist. It is interesting

to remark at this point that based on the symmetry in the problem any MT configuration can be rotated around the z -axis with no energy cost. This seemingly trivial feature - the energetic degeneracy- is in fact the most distinctive and unusual property of a polymorphic chain. We consider the consequences in the following.

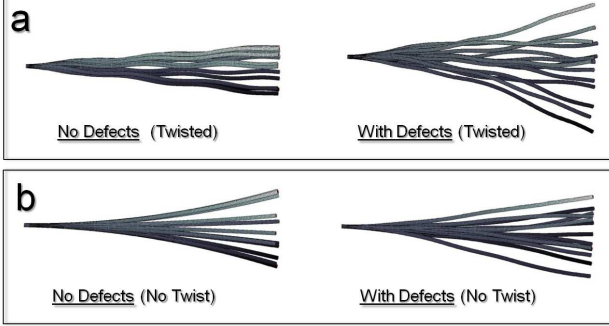


FIG. 8: The conical "wobbling" motion due to the rotational energy degeneracy of the polymorphic MT model : Snapshots of Monte-Carlo simulated lattice states. (a) Twisted MTs free of defects $L/l_\phi \ll 1$ and with numerous defects $L/l_\phi > 1$. For larger number of defects, the helix loses its coherent look. (b) For non-twisted MTs the movement has a typical parabolic "trumpet-like" shape.

The Wobbling Mode

By construction a polymorphic chain as we describe it here has a N fold symmetry. Therefore, there are N different helical states of different orientations with the same energy i.e. N ground states. This energy degeneracy is also reflected in the continuum model (where the N fold symmetry is approximated as continuous) by the rotational invariance of $E_{pol}(\phi)$ (which depends only on ϕ'). The broken cylindrical to helical symmetry of the straight state is then restored by the presence of a "Goldstone mode" $\phi \rightarrow \phi + \phi_0$ consisting of a rotation of P by an arbitrary angle ϕ_0 in the material frame (cf. Figs. 2 and 3). This mode comes energetically for free and leads to dramatic effects on chain's fluctuations. For instance for a MT clamped at one end, this symmetry implies that the MT will randomly rotate much like a rigid rotor as shown in Fig. 4. Note however that this rotation will still be associated with a certain dissipation as the system has to go over energy barriers between two helical states. This barrier due to the flipping of lattice states can be overcome at nonzero temperatures by the creation of double defects which diffusively propagate along the MT and eventually angularly reorient the polymorphic order parameter \vec{P} . These dynamic phenomena and the dissipation mechanisms will be discussed in a later section.

In summary, the zero-energy mode that we will also call the "wobbling mode" is an inherent feature of a helically polymorphic filament and as we will see now could be the culprit causing anomalous fluctuations of clamped MTs.

Persistence Length Anomalies

Among several definitions of the persistence length, we consider here - for direct comparison with clamped MTs experiments [37, 38] - the "lateral fluctuation persistence length" defined as

$$l_p^*(s) = (2/3) s^3 / V(s) \quad (15)$$

with $V(s) = \langle \rho(s)^2 \rangle - \langle \rho(s) \rangle^2$ the variance of $\rho^2 = x^2 + y^2$ - the transverse displacement at position s and $\langle \dots \rangle$ the ensemble average. We assume as in experiments [37, 38] a rigid clamping point at the position $s = 0$ preventing the microtubule from translating and rotating at that point.

For an ideal semiflexible wormlike chain we expect that the persistence length $l_p^* = l_B$ is a position independent and definition invariant quantity equal to the bending persistence length $l_B = B/k_B T$. (For another more classical definition of the persistence length - coming from the tangent correlation function, see also Appendix C). However for a polymorphic chain the strict equivalence of l_p^* and l_B is not correct. To see that, we can decompose the polymorphic and elastic fluctuations $\vec{\rho}(s) = \vec{\rho}_{pol} + \vec{\rho}_{el}$. Inserting this in Eq. 15 and taking into account that for small deflections the two components decouple $\langle \vec{\rho}_{pol} \vec{\rho}_{el} \rangle = 0$ leads us to the following relation for the persistence length

$$l_p^* = \left(l_{pol}^{-1} + l_B^{-1} \right)^{-1} \quad (16)$$

with the polymorphic persistence length given by $l_{pol} = (2/3) s^3 / V_{pol}$ and $V_{pol} = \langle \rho_{pol}^2 \rangle - \langle \rho_{pol} \rangle^2$. The average $\langle \dots \rangle$ is now performed over the phase ϕ governed by the energy Eq. 11. More precisely, the average of any arbitrary functional $A[\phi]$ of the polymorphic phase can be performed by first selecting one of the equivalent ground states denoted ϕ_0 characterized by $\phi(0) = \phi_0$ and performing the average over the polymorphic angle distribution Eq. 11 around the chosen ground state, i.e.,

$$\langle A[\phi] \rangle |_{\phi_0} = \frac{1}{Z} \int D\tilde{\phi} A[\tilde{\phi} + \phi_0] \exp\left(-\frac{l_\phi}{2} \int_0^L ds \tilde{\phi}'^2\right) \quad (17)$$

where $\tilde{\phi} = \phi - \phi_0$ (and thus $\tilde{\phi}(0) = 0$) and $Z = \int D\tilde{\phi} \exp\left(-\frac{l_\phi}{2} \int_0^L ds \tilde{\phi}'^2\right)$ is the partition function. In a second step - for a freely rotating polymorphic phase- we integrate over the rotational zero mode ϕ_0 : $\langle A[\phi] \rangle = \frac{1}{2\pi} \int \langle A[\phi] \rangle |_{\phi_0} d\phi_0$. This operation correctly takes into account the phase fluctuations over (and around) all

equivalent ground states related by the transform $\phi \rightarrow \tilde{\phi} + \phi_0$. The rotational symmetry around the z-axis (integration on ϕ_0) readily implies $\langle \rho_{pol}(s) \rangle = 0$ and $\langle x_{pol}^2 \rangle = \langle y_{pol}^2 \rangle$. Therefore the polymorphic persistence length can be written as

$$l_{pol}(s) = (1/3) s^3 / \langle y_{pol}^2(s) \rangle. \quad (18)$$

with

$$\langle y_{pol}^2(s) \rangle = \int_0^{2\pi} \frac{d\phi_0}{2\pi} \int_0^s \int_0^s \langle \theta_{y,pol}(s_1) \theta_{y,pol}(s_2) \rangle |_{\phi_0} ds_1 ds_2 \quad (19)$$

whose computation (for details cf. Appendix C) leads to the following mean square displacement

$$\langle y_{pol}(s)^2 \rangle = \frac{2\kappa_0^2 l_\phi}{3(1 + 4l_\phi^2 q_0^2)^4} \left\{ P_1(s) - e^{-\frac{s}{2l_\phi}} P_2(s) \cos(q_0 s) - e^{-\frac{s}{2l_\phi}} P_3(s) \sin(q_0 s) \right\} \quad (20)$$

where $P_i(s)$ are polynomial functions given in Appendix C.

A typical curve of l_p^* vs s is provided in Fig. 9. In general it shows three different characteristic regimes denoted I, II and III in the figure :

I. At short distances to the attachment point $s < s_{\min} \approx \pi/q_0$ (half the polymorphic wavelength) the total persistence length can be approximately given by

$$l_p^* \approx l_B - \frac{3\kappa_0^2 l_B^2 s}{8} \quad (21)$$

In the limit of very short distances $s \ll l_B^{-1} \kappa_0^{-2}$, the polymorphic fluctuations become negligible and are completely dominated by purely "classical" semiflexible chain fluctuations. Not surprisingly the persistence length coincides then with the classical bending persistence length $l_p^*(0) = l_B$. Starting from l_B , polymorphic fluctuations begin to contribute reducing l_p^* that attains a global minimum at $s_{\min} \approx \pi/q_0$.

II. For intermediate length values $s_{\min} < s < l_\phi$, the total persistence length displays a non-monotonic oscillatory behavior around a nearly linearly growing average

$$l_p^*(s) \approx \frac{2}{3} \frac{q_0^2}{\kappa_0^2} s + \frac{4}{3} \frac{q_0}{\kappa_0^2} \sin(q_0 s) \quad (22)$$

This result is worth deeper understanding. A moment of thinking reveals that the oscillatory part with wavelength $2\pi/q_0$ is related to the helicity of the ground state. At the same time the linear growth $l_p^*(s) \propto \alpha^2 s$ can be associated with the roughly conical rotation of the clamped chain (wobbling mode) which acts as an effective "rotational hinge" at the attachment point, cf. Fig. 4. The sinusoidally modulated rotation cone which builds an approximate envelope for the chains' motion has an opening

angle α which is related to the geometric features of the helix $\alpha = 2\kappa_0 q_0^{-1}$.

III. Finally for very large distances from the attachment point $s \gg l_\phi$ we expect to recover classical results of a semiflexible chain again. Indeed in this asymptotic regime the effective persistence length reaches saturation with a renormalized constant value $l_p^*(\infty) = 1 / (l_{pol}^{-1} + l_B^{-1})$ where

$$l_{pol} = 2l_\phi q_0^2 \kappa_0^{-2} + \frac{1}{2} \kappa_0^{-2} l_\phi^{-1} \quad (23)$$

Intuitively the helix loses then its "coherent nature" - due to strong variations of ϕ' and elastic fluctuations θ_{el} - and the collective rigid rotational ("conical") motion is finally replaced by an uncorrelated segment movement. Not surprisingly the persistence length becomes then length independent again. Curves for different values of l_ϕ are provided in Fig. 10.

Untwisted MTs

While there are no completely twist-free MTs and every lattice will have generically a small twist, one can still formally study the interesting limiting case $q_0 = 0$. Note that the large estimated pitch of 13PF MTs is finite and in the range of $\gtrsim 25\mu m$ [11–13, 15] while often assumed to be approximately infinite. In such an ideal case the theory still applies, however the overall behavior of $l_p^*(L)$ will substantially change and become much less consistent with the linear scaling found in experiments. While for $q_0 L > 1$ the chain in leading order moves on a linear cone (with fixed opening angle α) for $q_0 L \ll 1$ while still $L \ll l_\phi$ the "wobbling" motion is happening on a quadratic cone (a "trumpet shaped" cone, cf. Fig. 8b). More precisely for the exceptional case of untwisted MTs the polymorphic part of the lateral fluctuations Eq. 20 behaves as $\langle y_{pol}(s)^2 \rangle = 2/3\kappa_0^2 l_\phi (P_1 - e^{-\frac{s}{2l_\phi}} P_2)$ with $P_1(s) = 24l_\phi^3 - 3l_\phi s^2 + s^3$, $P_2(s) = 24l_\phi^3 + 12l_\phi^2 s$. Therefore for short MTs $L \ll l_\phi$, the lateral fluctuations grow with the length in fourth power $\langle y_{pol}(L)^2 \rangle \approx \kappa_0^2 L^4 / 8$, whereas for long ones $L \gg l_\phi$, the deviation grows cubically, $\langle y_{pol}(L)^2 \rangle = 2/3\kappa_0^2 l_\phi L^3$. From this, the persistence length has consequently two typical regimes. For $L \ll l_\phi$ we deduce from Eqs. 16 and 18 that $l_p^*(L) \approx (l_B^{-1} + 3/8\kappa_0^2 L)^{-1}$. The latter expression implies that long, untwisted MTs appear increasingly softer with growing length, and the effective persistence length decays inversely $l_p^* \propto 1/L$ for $L \gg 1/(3/8\kappa_0^2 l_B)$ and reaches a limiting value $l_p^* = l_B / (1 + 2l_B l_\phi \kappa_0^2)$ for $L \gg l_\phi$. For a MT of $L \sim 10 - 20\mu m$ we would expect $l_p^* \sim 10 - 20\mu m$ - a value 2 orders of magnitude smaller than observed in [37, 38]. This decreasing behavior is in contrast with observations $l_p^* \propto L$ - leading us to the

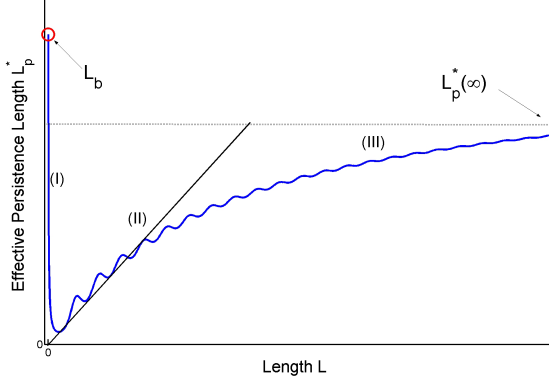


FIG. 9: A typical shape of the effective persistence length $l_p^*(L)$ for a clamped microtubule as obtained from Eqs. 16, 18 and 20. Most generically the curve displays three different regimes: (I) An initial rapidly decreasing regime where polymorphic effects become more effective with growing L (softening the chain), (II) a linearly-growing oscillatory regime - corresponding to the coherent wobbling movement of the clamped microtubule, (III) an asymptotic plateau regime, where the helix progressively loses its coherence with growing L . In this regime, the behavior tends to that of a classical semiflexible chain yet with a renormalized effective persistence length given by cf. Eq. 23.

conclusion that the 0-twist MTs does not constitute a significant portion of the experimental data [37, 38] and twist is necessarily required for the growth of l_p^* with L .

Having developed some static consequences of the polymorphic MT we now turn to its dynamical aspects.

Polymorphic Phase Dynamics

To describe the MT fluctuation dynamics we consider the total dissipation functional $P_{diss} = P_{ext} + P_{int}$ which is composed of an internal dissipation $P_{int} = \frac{1}{2}\xi_{int} \int \dot{\phi}^2 ds$ (with $\dot{\phi} \equiv d\phi/dt$) coming from the flipping of lattice states and an external hydrodynamic dissipation $P_{ext} = \frac{1}{2}\xi_{\perp} \int \dot{\rho}^2 ds$ associated with the time variation of the MT deflection $\vec{\rho}(s, t) = (x(s, t), y(s, t))$. We assume that the friction constant (per unit length) ξ_{\perp} of the helical MT is approximately the friction constant $\xi_{\perp} = 4\pi\eta / (\ln(2L/R) - 1/2)$ of a long slender body of length L , (small) radius $R \ll L$ moving in a fluid with viscosity η at low Reynolds numbers. The time evolution equation of the phase variable $\phi(s, t)$ and the lateral displacement $y(s, t)$ (and $x(s, t)$) are given by the coupled Langevin equations

$$\frac{\delta E_{tot}}{\delta \phi} = -\frac{\delta P_{diss}}{\delta \dot{\phi}} + \Gamma_{\phi} \quad (24)$$

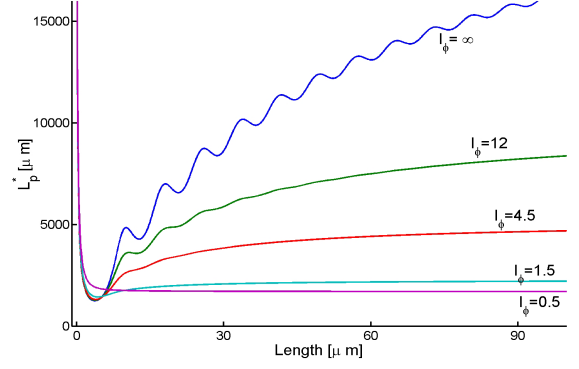


FIG. 10: Comparison of theoretical persistence lengths for different values of the polymorphic phase coherence length l_{ϕ} , ($l_B = 25mm$, $\kappa_0 = 0.03\mu m^{-1}$ and $q_0 = 0.8\mu m^{-1}$). For $l_{\phi} = \infty$, the MT is a (defect free) coherent helix performing the "wobbling motion" (as in Figs. 4 and 8a left panel). The plateau regime - where elastic fluctuations become dominant over polymorphic- is reached for very long MT only (not seen in the Fig.). Finite l_{ϕ} reduces the coherent wobbling motion - shortens region (II) of Fig. 9 - and the plateau regime is reached earlier with decreasing l_{ϕ} .

and

$$\frac{\delta E_{tot}}{\delta y} = -\frac{\delta P_{diss}}{\delta \dot{y}} + \Gamma_{\rho} \quad (25)$$

with $\Gamma_{\phi/\rho}$ the thermal noise terms. In general the lateral displacement $y(s, t)$ has contributions from both polymorphic $y_{pol}(s, t) \approx \kappa_0 \int_0^s ds' \int_0^{s'} \sin(\phi(\tilde{s}, t) + q_0 s) d\tilde{s}$ and elastic fluctuations $y_{el}(s, t) \approx \int_0^s \theta_{el}(s', t) ds'$ and the dynamics is highly non-linear. In the regime $L \gg l_{\phi}$ where the helix loses its coherence one expects to retrieve the dynamics of the usual semiflexible filament with $\tau \sim L^4$. However in the opposite and physically more interesting regime $L \ll l_{\phi}$ a new and different dynamic behavior can be expected. As we learnt from the study of the static case the effects of polymorphism become more pronounced at shorter lengths. As we have seen in this regime, the dominant motion is the wobbling rotation of a coherent helix on a cone where elastic fluctuations become negligible compared to polymorphic ones i.e. $y(s, t) \approx y_{pol}(s, t)$. In this regime few polymorphic defects $L \ll l_{\phi}$ are present and the phase can be approximated as $\phi(s, t) \approx \phi_0(t) + \delta\phi(s, t)$. Using this decomposition with $\delta\phi(s, t) \ll 1$ we can expand P_{ext} to leading order

$$P_{diss} \approx \frac{1}{2}L(\xi_{int} + \xi_{ext})\dot{\phi}_0^2 + O(\delta\dot{\phi}^2) \quad (26)$$

with a external friction constant ξ_{ext} given by

$$\xi_{ext} = \frac{\xi_{\perp} \kappa_0^2}{q_0^4} (2(1 + \cos Lq_0) - 4\frac{\sin Lq_0}{Lq_0} + \frac{q_0^2 L^2}{3}) \quad (27)$$

The evolution of the zero mode $\phi_0(t)$ reduces from the Langevin equation, Eq. 24, to $0 = -\frac{\delta P_{diss}}{\delta \phi_0} + \Gamma_\phi$ which leads to the equation of motion

$$\frac{d}{dt}\phi_0(t) = \frac{1}{\xi_{tot}}L^{-1}\int_0^L\Gamma_\phi(s,t)ds \quad (28)$$

with a friction constant $\xi_{tot} = \xi_{int} + \xi_{ext}$. Therefore $\phi_0(t)$ satisfies the simple Langevin equation Eq. 28 corresponding to a simple potential free Brownian motion with its mean square displacement given by (see Appendix D for a more detailed explanation)

$$\langle(\phi_0(t) - \phi_0(0))^2\rangle = \frac{2k_B T}{L\xi_{tot}}t. \quad (29)$$

In this limit (wobbling mode dominant) we have a roughly rigid helix moving randomly along a cone and all the physics is contained in the effective friction coefficient $\xi_{tot}(\xi_{int}, \kappa_0, q_0, L)$ and its dependence on the internal dissipation ξ_{int} , the helix parameters κ_0, q_0 and the length L .

For later comparison with experiments we compute the longest relaxation time τ given by the auto-correlation function $\langle y_{pol}(s,0)y_{pol}(s,t)\rangle \propto e^{-t/\tau}$. Using Eq. 29, a short computation (Appendix D) leads to

$$\langle y_{pol}(L,0)y_{pol}(L,t)\rangle = \langle y_{pol}^2(L)\rangle e^{-t/\tau(L)} \quad (30)$$

with $\langle y_{pol}^2(L)\rangle = \frac{\kappa_0^2}{q_0^2}\left(\frac{L^2}{2} + \frac{1-\cos(q_0L)}{q_0^2} - \frac{L\sin(q_0L)}{q_0}\right)$ the static mean square displacement Eq. 20 in the limit $L \ll l_\phi$ and with $\tau(L) = L\xi_{tot}/k_B T$ the longest relaxation time - proportional to the total friction constant ξ_{tot} - inheriting its length dependence in two different length regimes. For very short lengths $L \ll l_c = (3\xi_{int}\xi_\perp^{-1})^{1/2}q_0\kappa_0^{-1}$ when the hydrodynamic dissipation is entirely dominated by internal dissipation we have a linear scaling

$$\tau(L) \approx L\xi_{int}/k_B T. \quad (31)$$

For larger $L > l_c$ the wobbling movement through the fluid is the dominant source of dissipation and

$$\tau(L) \approx L\xi_{ext}(L)/k_B T. \quad (32)$$

with $\xi_{ext}(L)$ given by Eq. 27. Note that the L dependence of ξ_{ext} relies also on the L dependence of $\xi_\perp(L)$ which for simplicity has been modelled as the friction of an ideal slender tube moving in a liquid. A more precise (but difficult) determination of ξ_\perp could slightly change its variation with L , although not the general trends of $\xi_{ext}(L)$. In particular if we assume that ξ_\perp is L independent and that $Lq_0 \gg 1$ we have in this regime the scaling

$$\tau(L) \approx \frac{\xi_\perp}{3k_B T}(\kappa_0/q_0)^2 L^3. \quad (33)$$

So in summary for τ we expect a cross-over from a linear, internal dissipation dominated L dependence at short lengths to a cubic length dependence given by hydrodynamic friction alone.

COMPARISON WITH CLAMPED MT EXPERIMENTS

The comparison with experiments [37, 38] which measure lateral fluctuations of clamped MTs reveals several interesting characteristics that are in agreement with predictions, cf. Fig. 11. First, the predicted mean linear growth of $l_p^*(L)$ agrees with experiments as a single exponential fit $l_p^* \sim L^\delta$ of the data provides $\delta = 1.05$. Besides the linear growth the experimental data reveal a large spread of l_p^* data points which seems to grow approximately in proportion to the length. This linearly growing experimental spread is likely linked to the intrinsic spread of q_0 values of different MT lattice populations [11–13, 15]. MTs with different number of protofilaments will display different lattice twists ranging from $q_0 \approx 2\pi/3\mu m$ (for 12 PF MTs) to $q_0 \lesssim 2\pi/25\mu m$ (for 13 PF MTs). Keeping in mind the scaling $l_p^*(s) \propto q_0^2 s$ (cf. Eq. 22) we would expect more than an order of magnitude variation of measured l_p^* while the slope $l_p^*(s)/s$ should display a constant spread.

Second, the data of Taute et al. [38] (Fig. 11, circle) indicate a non-monotonic dependence with systematic trends over several consecutive data points. This seems phenomenologically well captured by the oscillatory behavior $l_p^*(L)$ from Eq. 22. On the other hand, the data of Pampaloni et al. [37] are definitely much more spread and don't allow such a clear conclusion. Therefore the non-monotonicity of $l_p^*(L)$ is at present experimentally difficult to infer from the two existing experimental data sets taken together, however it is consistent with data within the error bars. As mentioned the presence of different lattice populations (even within single MTs) could give rise to a large spread of experimental data points and an effective "washing out" of the non-monotonic behavior for different lattices within the same statistics.

Remarkably the experimental data reveal that the large length plateau $s \gg l_\phi$ where l_p^* would become length independent is not reached even for longest MTs ($\sim 50\mu m$). This is in phenomenological agreement with the theory - as based on the observed long coherent helices by Venier et al [27] it would imply a very long l_ϕ . The absence of the plateau in Pampaloni and Taute's data allows a lower estimate of the coherence length: $l_\phi > 55\mu m$ which in turn would imply a large coupling constant $J > 4k_B T$. The best comparison between theory and experiments (cf. Fig. 11) gives $l_B = 25mm$ corresponding to a rather high Young modulus $Y \approx 9GPa$ higher than typically reported before [26–32, 39, 40]. However the present value is well within the range for

proteins and protein tubes with Y up to $19GPa$ are reported in literature [57]. The higher value of the bare Young modulus extracted from the present theory should also not be a surprise as in previous models all MT conformational fluctuations were interpreted as originating from bending deformations alone. In our model - both elastic and polymorphic fluctuations contribute with the latter being much softer and giving therefore dominant contribution.

The best fitting helix wave length $\lambda \approx 7.5\mu m$ is close to the expected $6\mu m$ corresponding to the twist [11–13, 15] of the 14 PF MT population. This is in agreement with the fact that, - in contrast to the in vivo situation- the large pitch ($\lambda \approx 25\mu m$) 13PF MTs are likely underrepresented in the data [37, 38]. Indeed in vitro studies of taxol-copolymerized MTs display a MT population consisting of a majority of 14 PFs (61%) while 13 PFs (32%) are less represented [11–13, 15]. The in vitro conditions therefore strongly shift the PF population away from the preferred low twist 13 PF MT towards the highly twisted 14PF MT.

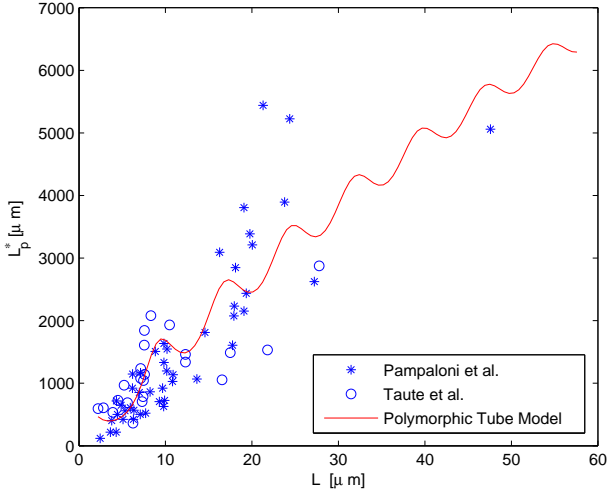


FIG. 11: Effective persistence length l_p^* as a function of the position from the attachment point along the clamped MT contour. The experimental data (stars and circles) [37, 38] and the theoretical prediction with $l_B = 25mm$, $\lambda = 7.5\mu m$, $\kappa_0^{-1} = 18\mu m$, $q_0 l_\phi \gg 1$.

The estimated l_B is larger than in previous studies ($l_B \sim 1 - 6mm$) where however polymorphic fluctuations were neglected. This result leads us to the conclusion that if polymorphism is partially suppressed one would measure much larger effective l_p - as in fact observed. For example in studies where 2D slab geometry is used (MTs between 2 close glass slides) an effective suppression of the 3 dimensional polymorphic helices or their reduced mobility is expected. A typical observation in such cases is an extensive “intrinsic curvature” (of previously un-

known origin). Within our theory one could interpret this curvature as pinned / quenched polymorphic helices prevented from free fluctuations by the confinement. These effects could in general explain the dramatic variations of measured l_p values based on the presence/ absence of polymorphic “softening” in different experimental setups and geometries.

Now, let us consider the clamped MT dynamics as investigated in [38]. A careful analysis of Taute et al’s data reveals a peculiar scaling of the longest relaxation time with the length. Indeed an independent single exponent fit of the Taute et al data [38] gives $\tau \propto L^\alpha$ with $\alpha = 2.9$ in the experimental range considered $2.2\mu m < L < 28\mu m$. This peculiar scaling can be understood as originating from hydrodynamic relaxation of a “wobbling” polymorphic chain. Using only the previously best fitting parameters of the static data (Fig. 11) $(\kappa_0/q_0)^2 \approx 4.8 \times 10^{-3}$ and $\eta = 10^{-3} Pa \cdot s$ (water viscosity) we find a remarkable correspondence between the theoretical prediction Eq. 32, i.e., $\tau_{th}(L) \approx L\xi_{ext}(L)/k_B T$ and data of [38], as shown in Fig. 12. This 0-parameter prediction matches well the data for larger lengths. For scaling comparison, it is interesting to compare the data with the approximate theoretical relaxation time Eq. 33, i.e., $\tau(L) \approx \frac{\xi_\perp}{3k_B T} (\kappa_0/q_0)^2 L^3$ (expression strictly valid for $L \gg 0.8 \mu m$) which has a scaling law in agreement with the single exponent fit of the data. Considering that $\xi_\perp \approx 1.6\eta - 2.3\eta$ is roughly length independent in the experimental L range one can assume $\xi_\perp \approx 2\eta$ and obtains the prefactor $\tau_{th}/L^3 = 7.9 \times 10^{14} s/m^3$. Keeping in mind the simplicity of the interpretation (and the lack of free parameters therein), this compares very favorably with the best fit of experimental data slope $\tau_{fit}/L^3 = 6.25 \times 10^{14} s/m^3$ (cf. Fig. 12). Note that the approximate value of τ_{th} seems to correspond a little better to the data but this is likely of no physical significance at this level of approximation. Indeed the neglected elastic modes other than the wobbling as well as the approximation of the hydrodynamic friction should change the details of the L dependence of ξ_{ext} and thus of τ_{th} (but not the general trends). Without a more precise computation of the dynamics we can be satisfied with the rather astonishing agreement between theory and experiment for long MTs. This leads us again to the conclusion that in these experiments long MTs behave as almost rigid helical polymorphic rotors whose motion is dominated by the zero energy “wobbling” mode and its hydrodynamic dissipation[62].

For very short MTs we should expect deviation from this simple interpretation. In this regime the linearly scaling internal dissipation, coming from the migration of polymorphic defects, should start to dominate over pure hydrodynamic friction and for sufficiently short MT lengths $L \rightarrow 0$ we could measure ξ_{int} from the limit value of τ_{th}/L . It appears that for the presently available data $L > 2 \mu m$ [38] this plateau-regime is not yet fully de-

veloped, enabling us to provide only an upper numerical estimate for the inner dissipation $\xi_{int} \lesssim 4 \times 10^{-17} Ns$.

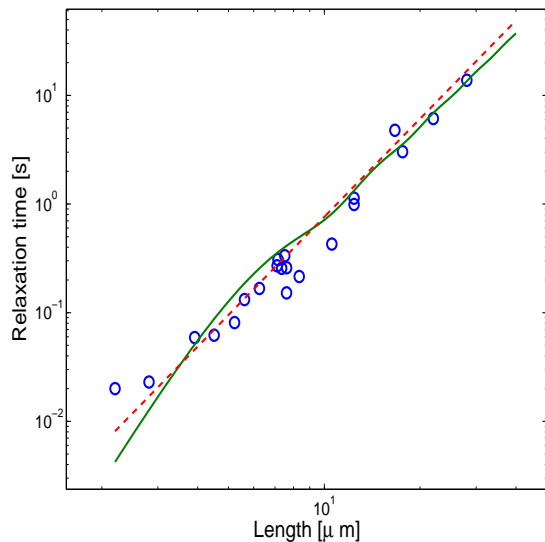


FIG. 12: The experimental microtubule relaxation times [38] and the no-adjustable-parameter theoretical prediction (full line) as obtained from static data in Fig.11 (with $l_B = 25mm$, $\lambda = 7.5\mu m$, $\kappa_0^{-1} = 18\mu m$, $q_0 l_\phi \gg 1$). The dashed line illustrates the long length approximation Eq. 33 displaying the characteristic cubic scaling with length.

Very Short MTs

Comparison with experiments for even shorter chains ($L < \pi/q_0$) is more difficult due to the lack of data in clamped MT experiments ($L > 2\mu m$). We can nevertheless try a comparison with the results by the Dekker group for the kinesin motor gliding assay of short MTs [34, 35]. Besides some similarities with the clamped fluctuating MTs, there are a number of differences between the modelled situation of free 3D MTs and the 2D gliding assay. In particular the 2D geometry will strongly perturb the preferentially 3-dimensional helical ground state. The active contribution of strong motor forces on the trajectory of short MTs is an additional potential perturbation. Effects of MT buckling and axial MT rotation by kinesins become likely important. This said and ignoring the differences we can still compare (in order of magnitude) our and Dekker groups' results [34, 35]. For micron sized MTs we obtain $l_p \sim 0.8\mu m$ in approximate agreement with $\sim 0.2\mu m$ obtained in [34]. One should mention that the two cited studies [34, 35] give strongly different results depending on whether free gliding or gliding assay with additional electric field were considered. This difference comes from the larger deformations induced by the electric field. Therefore the

comparison of our theory with the passive gliding assay appears more appropriate and gives a closer agreement.

SUMMARY

In summary, we have suggested a new model that connects some of the most persistent and confusing experimental findings concerning microtubules. Starting from a rather broad spectrum of (apparently) disconnected observations we have progressively built the case for a new hypothesis : the existence of an internal switching of the GDP tubulin dimer within the microtubule lattice. Why do microtubules become helically wavy, why do they switch to permanently bent circular states, why do they fluctuate anomalously when clamped? These three dangling questions became the central pillars for the present model. Surprisingly, the simple assumption of a bistable GDP-tubulin seems to explain these otherwise disparate phenomena in a unified manner. As we know from recent experiments - the bistability hypothesis of taxol stabilized protofilaments is an empirical fact indeed [25]. We have shown here, that the incorporation of such a bistable tubulin into a closed elastic lattice changes its free behavior - it introduces strong conformational competition among the tubulin dimers. Tubulin units on opposite sides of the tube now start to compete for who is going to switch to the curved state. The lattice induced frustration does not allow all the tubulin dimers to minimize their energy individually and to switch to their preferred states at the same time. The symmetry breaking induced by this frustration mechanism leads to a global microtubule lattice curving. Remarkably the curving direction is chosen randomly - and this has profound consequences. The microtubule can chose between many energetic ground states (as many states as protofilaments in the lattice). When we graft one end of the microtubule onto a substrate while still allowing it to chose its bending direction freely the strange energy degeneracy generates a very unusual thermal motion. In this case the microtubule's motion follows -roughly speaking- a cone and it rotates - or "wobbles"- at no energy cost around its attachment tangent. This mode of motion - which is not to be confused with material frame rotation (which is strictly prohibited by grafting) - is probably among the most striking outcomes of the two state GDP-tubulin model. It is exactly this behavior that allows to consistently explain the measurements of unusual lateral fluctuations of grafted microtubules [37, 38].

PERSPECTIVES

We have focussed here on modelling taxol stabilized microtubules and the question naturally arises if the model proposed here affects the 'real' in vivo micro-

tubules. On the one hand the 'weakly curved' state that is involved in the soft polymorphic dynamics as described here seems to be (so far) a specific signature of taxol stabilized GDP tubulin state. On the other hand we have argued that the naturally occurring 'high curvature' GDP-tubulin state could coexist with the straight state in the lattice under *in vivo* conditions where MTs are stabilized with MAPs. The involvement of this 'high curvature' state switching seems to manifest itself in motor driven straight to wavy transitions of MTs in many living cell systems [39, 48–52]. A particularly impressive instance of such a polymorphic switching event *in vivo* could be found in the process of axonal retraction where the whole MT cytoskeleton of the axon undergoes a straight to helical transition and in turn retracts towards the soma [54]. To understand these dramatic transitions *in vivo* the present theory has to be advanced and modified in two manners. First, the effect of large active motor forces (rather than thermal ones) has to be taken into account. In particular, one expects that under strong buckling forces even thermodynamically unfavorable states can become activated and constitute the ground state upon large loads.

Second, in virtually all *in vivo* experiments MTs are essentially confined in 2D as the containing cells adsorb to the glass substrate and assume a vary flat 'fried egg' configuration. Consequently, the measured properties will not necessarily reflect the three-dimensional properties of the molecule. This is particularly important for a MT transformed to a polymorphic helix state where the confinement entails naturally a strong deformation (of the initially 3 dimensional ground state). Under confinement the helical bending and torsional modes become strongly coupled and bring about new physical effects. In particular a torsionally very soft helix will have a tendency to unwind and form in extreme cases circular arcs - reminiscent of the rings observed in gliding assay experiments [42].

Finally, the local action of molecular motors could trigger a switching to the highly curved state. While for classical motors like kinesin 1 direct evidence for such a mode of action is still missing its relative kinesin 13 [25, 58] has a well documented ability to actively trigger radial bending of protofilaments. Other molecules like katanin [59, 60] have also been suggested to perturb the lattice and trigger longer range transitions [46]. This opens the intriguing question : could classical motors (kinesin 1 and dynein) trigger cooperative state transitions and even transmit conformational signals along the tube? Considering the present model for stabilized MTs (where high cooperativity is inherent to the data interpretation) this idea might not be far fetched. In fact some evidence towards long range cooperativity of kinesin binding along the MT was presented by Muto et al. [61] - however these results still await robust reproduction.

This brings us to the question of what experiments

should be performed in order to nail down the polymorphic mechanism or any other mechanism for MT dynamics. With microtubules being such delicate, subtle and possibly long range correlated objects (as suggested here) a general rule of thumb for experiments should be: Treat them more gently (do not confine) and observe more carefully (look for correlated motion). A simple yet important experiment would be a systematic *direct* observation of one-side grafted but otherwise *completely unconfined* MTs fluorescently labelled *along their full contour length*. As mentioned the presence of a quasi 2D confinement in thin chambers as used in most MT experiments so far would perturb the native helical MT state and should be therefore explicitly avoided. The freely suspended gold-EM nanogrid attachment geometry as used by Pampaloni et al. seems particularly suited for that task. Going beyond Pampaloni et al. who labelled and traced the MT end only (via a bead), the microtubules should be visualized along the full contour in this geometry. Tracing of several or all points along the contour should reveal the predicted sinusoid- helical nature of MT states. The present model predicts a peculiar cooperatively rearranging helix state with characteristic tell tale curvature correlations between different lattice positions which are entirely absent for usual semiflexible filaments. Directly observing such collective motions - like the suggested "wobbling mode" - while prohibiting trivial spacial rotations that could mask the effects (by MT grafting) would constitute smoking gun evidence for a polymorphism related mechanism.

In conclusion, we have proposed a novel model for internal MT lattice dynamics. We have shown that it accounts for the otherwise mysterious MT helicity [27], the anomalous length dependent lateral fluctuation static [37, 38] and dynamic scaling [38]. The latter two phenomena appear as mere consequences of the peculiar "wobbling motion" of the polymorphic cooperatively switching MT lattice. Although most of the observations discussed here are made *in vitro* on taxol-stabilized MTs, we provided arguments in favor the existence of polymorphic MT states *in vivo*. We speculate that the implied conformational bistability of tubulin and the allosteric interaction are more than just nature's way to modulate the elastic properties of its most important cytoskeletal mechano-element. It could also be a missing piece in the puzzle of polymerization "catastrophes". Even more intriguingly the predicted structural cooperativity could allow for long range conformational signalling along single MTs and turn the latter into an efficient "confotronic" wire transmitting regulatory signals across the cell.

ACKNOWLEDGEMENTS

We acknowledge fruitful discussions with Francesco Pampaloni, Denis Chrétien, Thomas Surrey, Francois

Nédélec, Jean-Francois Joanny, Sergey Obukhov, Linda Amos, André E.X. Brown and thank Falko Ziebert for discussion and useful comments on the manuscript.

APPENDIX

A. Polymorphic phase coherence length

In this section, we derive the formula $l_\phi = \frac{N^2 b}{8\pi^2} (2 + e^{2J/k_B T})$ for the polymorphic phase coherence length. To this end we want to calculate the distribution of double junctions that leads to angular orientation change $\Delta\Phi$ on a scales l much larger than the tubulin dimer b , yet still much smaller than the total length: $b \ll l \ll L$. In this domain, at each cross section we have 3 possibilities:

- 1) State $j = 0$ with no double defect. The rotation angle $\Delta\Phi$ is attached to the internal lattice rotation, $\frac{\Delta\Phi}{b} - q_0 = 0$
- 2) State $j = -1$ for a left handed double defect, $\Delta\Phi$ deviates from the internal twist : $\frac{\Delta\Phi}{b} - q_0 = -\frac{1}{b} \frac{2\pi}{N}$
- 3) State $j = +1$ for a right handed double defect with $\frac{\Delta\Phi}{b} - q_0 = +\frac{1}{b} \frac{2\pi}{N}$.

On a length l we are throwing a 3 sided dice l/b times and the total rotation of $\Delta\Phi$ away from optimal twist is $\Delta\Phi - q_0 l = \frac{2\pi}{N} \sum_{n=1}^{l/b} j_n$. The variation of the polymorphic phase with respect to the internal twist is then

$$\Delta\phi = \frac{\Delta\Phi}{l} - q_0 = \frac{1}{l} \frac{2\pi}{N} \sum_{n=1}^{l/b} j_n$$

For $l/a \gg 1$ the law of large numbers implies that the random variable $\Delta\phi = \frac{1}{l} \frac{2\pi}{N} \sum_{n=1}^{l/b} j_n$ becomes Gaussian distributed

$$p(\Delta\phi) \propto e^{-\frac{\Delta\phi^2}{2\langle\Delta\phi^2\rangle}}$$

with mean $\langle\Delta\phi\rangle = 0$ and $\langle\Delta\phi^2\rangle = (\frac{1}{l} \frac{2\pi}{N})^2 (\frac{l}{b}) \langle j^2 \rangle$ (as $\langle j_n j_m \rangle = \delta_{nm} \langle j^2 \rangle$). The average $\langle j^2 \rangle$ is given from the Boltzmann factors of the three different states $p_0 = \frac{1}{1+2e^{-2\beta J}}$ and $p_{\pm 1} = \frac{e^{-2\beta J}}{1+2e^{-2\beta J}}$ so that $\langle j^2 \rangle = \frac{2e^{-2\beta J}}{1+2e^{-2\beta J}}$. We can now interpret the quantity $1/(2\langle\Delta\phi^2\rangle)$ as coming from an effective elastic energy over the interval l by writing $\frac{\Delta\phi^2}{2\langle\Delta\phi^2\rangle} = \frac{1}{2} \beta C_\phi l (\Delta\phi)^2$ which allows us to identify the effective stiffness

$$C_\phi = kT \frac{N^2}{8\pi^2} (2 + e^{2J\beta}) b.$$

Note that this expression is valid for large enough J suppressing higher order defects i.e. in the limit when multiple double defects sitting on a single lattice site (i.e. $|j| > 1$) can be ignored.

B. The variation of the polymorphic modulus

In this appendix we compute the energy variation due to a deviation of the polymorphic modulus $|P|$ away from its optimal value $|P^*|$ minimizing the energy; i.e., the change of the number of switched PFs. We start with the energy density of a MT cross section

$$e = \frac{B}{2} \left((\kappa - \kappa_{pol}(p))^2 + \kappa_1^2 \left(\gamma \frac{\pi}{N} p - \sin^2 \left(\frac{\pi}{N} p \right) \right) \right) \quad (34)$$

whose minimum energy is reached for $p^* = \frac{N}{2} - \frac{N}{2\pi} \arcsin \gamma$. Assuming a continuous number of PFs, the energy of a state with $p = p^* + \Delta p$ switched PFs reads to quadratic order:

$$\begin{aligned} e(p^* + \Delta p) &\approx e(p^*) - \frac{\pi^2 B}{N^2} \kappa_1^2 \cos \left(\frac{2\pi}{N} p^* \right) \Delta p^2 \\ &= e(p^*) + \frac{\pi^2 B}{N^2} \kappa_1^2 \sqrt{1 - \gamma^2} \Delta p^2 \end{aligned}$$

where we used $\cos(\pi - \arcsin \gamma) = -\sqrt{1 - \gamma^2}$. Therefore the energy variation of a segment of length l reads

$$\Delta E \approx \frac{\pi^2 B}{N^2} \kappa_1^2 \sqrt{1 - \gamma^2} \int_0^l ds (p(s) - p^*(s))^2$$

Now using $|P(s)| = |\sin(\frac{\pi}{N} p)| / \sin(\pi/N)$ we can write the energy variation to the same (quadratic) order as

$$\Delta E \approx B \kappa_1^2 \sin^2(\pi/N) \sqrt{1 - \gamma^2} \int_0^l ds (|P(s)| - |P^*|)^2$$

Therefore any deviation of P from its optimum state P^* is associated with an energy cost proportional to the length l of the region in the unfavorable state.

C. Persistence length(s)

A definition of the persistence length, often used in single molecule experiments, is expressed in terms of the lateral deviation $\vec{p} = (x(s), y(s))$ of a MT clamped at $s = 0$ from its attachment axis : $l_p^*(s) = 2/3s^3 / \langle (\vec{p}(s) - \langle \vec{p}(s) \rangle)^2 \rangle$ and $\langle \dots \rangle$ is the statistical average. The equivalence of the x and y directions implies that $l_p^*(s) = 1/3s^3 / \langle (y(s) - \langle y(s) \rangle)^2 \rangle$. The second often used alternative but more standard definition of the persistence length - the tangent persistence length- is related to the angular correlation $l_p(s - s') = |s - s'| / V(s - s')$ with the variance $V = \langle (\theta_y(s) - \theta_y(s'))^2 \rangle$ (by symmetry we have the same expression with θ_x). Whereas for an ideal WLC $l_p^* = l_p = l_B$ is position and definition independent this is not the case for a polymorphic chain (see Fig. 13). For small angular deformations the decoupling of chain's fluctuations

into polymorphic and purely elastic contributions allows to decompose the persistence length as $l_p^{-1} = l_{pol}^{-1} + l_B^{-1}$ - this result being valid for both definitions of the persistence length.

We first focus on the first definition - the clamped persistence length. In this case the polymorphic persistence length $l_{pol}^*(s)$ is given by

$$l_{pol}^*(s) = 1/3s^3 / \langle (y_{pol}(s) - \langle y_{pol}(s) \rangle)^2 \rangle \quad (35)$$

where $y_{pol}(s)$ is the lateral polymorphic displacement in the y direction. Integrating over the rotational zero mode readily implies $\langle y_{pol}(s) \rangle = 0$ (see Eq. 18). From Eq. 19 one can write

$$\langle y_{pol}^2(s) \rangle = \int_0^s \int_0^s G(s_1, s_2) ds_1 ds_2$$

with the angular correlation function $G(s_1, s_2) = \langle \theta_{y,pol}(s_1) \theta_{y,pol}(s_2) \rangle$ given by the integration over the zero mode

$$G(s_1, s_2) = \int_0^{2\pi} \frac{d\phi_0}{2\pi} G_0(s_1, s_2, \phi_0) \quad (36)$$

of the angular correlation function at fixed value of ϕ_0 , i.e., $G_0(s_1, s_2, \phi_0) = \langle \theta_{y,pol}(s_1) \theta_{y,pol}(s_2) \rangle |_{\phi_0}$. This last expression, from the relation $\theta_{y,pol}(s) = \kappa_0 \int_0^s \sin(\tilde{\phi}(s') + q_0 s' + \phi_0) ds'$ (cf. Eq. 17) is explicitly given by

$$G_0(s_1, s_2, \phi_0) = \kappa_0^2 \int_0^{s_1} \int_0^{s_2} \langle \sin(\tilde{\phi}(s) + q_0 s + \phi_0) \sin(\tilde{\phi}(s') + q_0 s' + \phi_0) \rangle |_{\phi_0} ds ds' \quad (37)$$

After integration over ϕ_0 and using the known result $\langle \cos(\tilde{\phi}(s_1) - \tilde{\phi}(s_2)) \rangle = e^{-|s_1 - s_2|/2l_\phi}$ which results from the WLC type probability distribution of the field $\tilde{\phi}$, i.e., $P[\tilde{\phi}] \sim \exp(-\frac{l_\phi}{2} \int_0^L ds \tilde{\phi}'^2)$ one obtains the rotational invariant correlation function in the form

$$G(s_1, s_2) = \frac{\kappa_0^2}{2} \int_0^{s_1} \int_0^{s_2} e^{-\frac{|s-s'|}{2l_\phi}} \cos(q_0(s-s')) ds ds' \quad (38)$$

Computation of the integrals in Eq. 38 gives finally the following expression for the polymorphic contribution of the transverse displacement

$$\langle y_{pol}(s)^2 \rangle = \frac{2\kappa_0^2 l_\phi}{3(1+4l_\phi^2 q_0^2)^4} \left\{ P_1 - e^{-\frac{s}{2l_\phi}} P_2 \cos(q_0 s) + e^{-\frac{s}{2l_\phi}} P_3 \sin(q_0 s) \right\} \quad (39)$$

with $P_1(s) = 24l_\phi^3 (1 - 6x + x^2) - 3l_\phi (1 + x - x^2 - x^3) s^2$

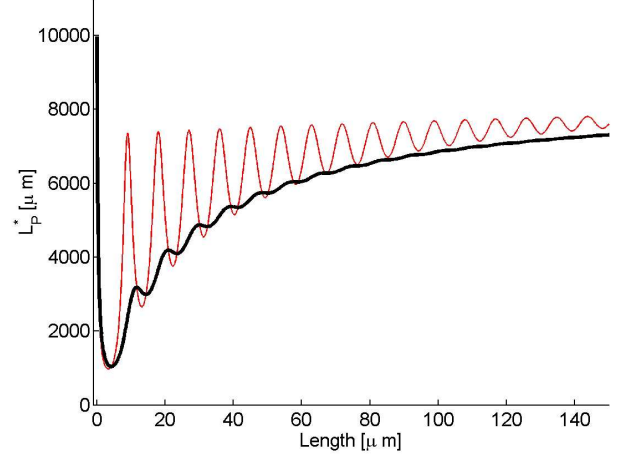


FIG. 13: Different definitions of the persistence length can deviate from each other for a polymorphic chain. The "clamped persistence length" l_p^* (thick line) and the "tangent persistence length" l_p (thin line) (for $l_B = 10mm$, $l_\phi = 50\mu m$, $\kappa_0 = 0.03\mu m^{-1}$ and $q_0 = 0.7\mu m^{-1}$).

$+ (1 + 3x + 3x^2 + x^3) s^3$, $P_2(s) = 24l_\phi^3 (1 - 6x + x^2) + 12l_\phi^2 (1 - 2x - 3x^2) s$ and $P_3(s) = 192l_\phi^4 q_0 (1 - x) + 24l_\phi^3 q_0 (3 + 2x - x^2) s$ where we have introduced the notation $x = 4l_\phi^2 q_0^2$.

From Eq. 39, we get the polymorphic persistence length $l_{pol}^*(s)$ defined in Eq. 35, and in turn the global persistence length $l_p^*(s)$ depicted in Fig. 13. Its physical interpretation is discussed in the main text.

We now consider the second definition of the persistence length $l_p(s-s') = |s-s'|/V(s-s')$. From Eq. 38, the angular variance V_{pol} can easily be evaluated

$$V_{pol}(s) = \frac{2\kappa_0^2 l_\phi}{1+4l_\phi^2 q_0^2} \left(s - \frac{2l_\phi (1-4q_0^2 l_\phi^2)}{1+4l_\phi^2 q_0^2} \right) + \frac{4\kappa_0^2 l_\phi^2 e^{-\frac{s}{2l_\phi}}}{(1+4l_\phi^2 q_0^2)^2} \left((1-4q_0^2 l_\phi^2) \cos(q_0 s) - 4q_0 l_\phi \sin(q_0 s) \right) \quad (40)$$

The resulting persistence length l_p (depicted in Fig. 13) shows a rich behavior similar to the persistence length $l_p^*(s)$ but displays a distinct functional form from the latter. However as expected, both curves reach the same asymptotic value at very short and very long MT lengths.

D. Zero mode dynamics

The evolution of the zero mode $\phi_0(t)$ is given by Eq. 28:

$$\frac{d}{dt}\phi_0(t) = \frac{1}{\xi_{tot}}L^{-1}\int_0^L\Gamma_\phi(s,t)ds \quad (41)$$

with a friction constant $\xi_{tot} = \xi_{int} + \xi_{ext}$ where ξ_{ext} is given by Eq. 27. The correlation function of the thermal white $\Gamma_\phi(s, t)$ noise is $\langle \Gamma_\phi(s, t)\Gamma_\phi(s', t') \rangle = D\delta(s - s')\delta(t - t')$ with a coefficient D that can be determined in the following manner. Notice first that ϕ_0 performs a free Brownian motion and its quadratic fluctuations necessarily satisfy the relation $\langle (\phi_0(t) - \phi_0(0))^2 \rangle = \frac{2k_B T}{L\xi_{tot}}t$. On another hand integrating Eq. 41 :

$$\phi_0(t) - \phi_0(0) = \xi_{tot}^{-1}\int_0^t\left(\frac{1}{L}\int_0^L\Gamma(s, t')ds\right)dt' \quad (42)$$

and averaging over the white noise the quadratic phase fluctuations one obtains : $\langle (\phi_0(t) - \phi_0(0))^2 \rangle = \frac{D}{\xi_{tot}^2}t$, from which we readily deduce $D = 2\xi_{tot}k_B T$ - as expected from the fluctuation dissipation theorem.

The relaxation time is generally given from the time correlation function $\langle y_{pol}(s, 0)y_{pol}(s, t) \rangle$ with the lateral position $y_{pol}(s, t) = \frac{\kappa_0}{q_0}(sq_0 \cos(\phi_0(t) + \alpha) + \sin(\phi_0(t) + \alpha) - \sin(q_0s + \phi_0(t) + \alpha))$ obtained from Eq. 14 with $l_\phi \gg s$. The average must first take into account all statistically equivalent values of angular orientations $\alpha \in [0, 2\pi]$, such that $\langle y_{pol}(s, 0)y_{pol}(s, t) \rangle = \int_0^{2\pi} \langle y_{pol}(s, 0)y_{pol}(s, t) \rangle_\alpha \frac{d\alpha}{2\pi}$ and we obtain

$$\langle y_{pol}(s, 0)y_{pol}(s, t) \rangle = \langle y_{pol}^2(s) \rangle \langle \cos(\phi_0(t) - \phi_0(0)) \rangle \quad (43)$$

with $\langle y_{pol}^2(s) \rangle = \frac{\kappa_0^2}{q_0^2} \left(\frac{s^2}{2} + \frac{1 - \cos(q_0s)}{q_0^2} - \frac{s \sin(q_0s)}{q_0} \right)$ corresponding to the static result Eq. 39 in the limit $s/l_\phi \ll 1$. With 42 defining a simple Gaussian random walk processes one straightforwardly obtains

$$\langle \cos(\phi_0(t) - \phi_0(0)) \rangle = e^{-t/\tau} \quad (44)$$

with the relaxation time given by

$$\tau = L \frac{\xi_{tot}}{k_B T}. \quad (45)$$

E. Comment on MT surface attachment and the robustness of "wobbling"

Throughout this work we have assumed that the free rearrangement of the polymorphic lattice states is not significantly hindered by the covalent surface attachment of the MT, as e.g. performed in [37] and [38]. This assumption is integral to the "wobbling" motion and in turn to understanding the static and dynamic data scaling. It therefore deserves a closer consideration.

In the experiments by Pampaloni [37] et al. and Taute et al. [38] the adsorbed MT part is attached to a gold (electron microscopy grid) surface via thiol groups. It is likely that $\approx 1 - 2$ protofilaments will establish localized chemical contacts with the gold microgrid. While a substantial perturbation of the dimer like e.g. denaturation appears unlikely, it is unclear to what extent this procedure will perturb the inner (polymorphic) dynamics of the entire tubulin dimer units. In principle one can anticipate two plausible scenarios that would to a varying degree interfere with the free "wobbling" motion:

S1) Due to high cooperativity (large coupling J) the polymorphic state transition can propagate within a certain penetration depth into the adsorbed (straight-planar) MT section.

S2) The cooperativity is too weak to compete with the constraints imposed by the surface (including chemical perturbations) and the polymorphic transition does not propagate into the straight adsorbed MT section.

In both cases we have a non vanishing deflection angle between a forced (adsorbed) planar section and the free helical section direction - causing effectively the characteristic MT "kink" at the surface interface. However the rotational mobility of this "kink" (wobbling mode) which is integral to our theory will be affected in slightly different manner.

If in case S1 in the adsorbed section the polymorphic order parameter P can rearrange to some extent (by switching the monomer states without causing a detectable deformation) except for possibly in the few surface interacting dimers, then the effects of the "wobbling" motion will be hindered only mildly in the following sense. To retrieve the anomalous lateral fluctuations it is indeed enough for the wobbling angle ϕ_0 to move freely in a certain non-vanishing angular interval. A single complete or multiple rotations of the order parameter \vec{P} are not strictly necessary for the "hinge" effect - and they are in fact equivalent in lateral projection (as in experiment) to the motion of the wobbling angle ϕ_0 in the smaller interval $[-\pi/2, +\pi/2]$. Note that even smaller intervals than that will lead to a similar phenomenology (in particular dynamic and static variable scalings with length). Thus the conical hinge-like motion is in a sense robust with respect to a limited local rotational hindrance perturbation in the adsorbed region.

In the scenario S2 the situation is somehow simpler as the polymorphic dynamics of the adsorbed region is not involved in the process (the polymorphic order parameter vanishes there: $\vec{P} = 0$). Wobbling is realized through a coherent rearrangement of the free MT section alone - without a strong coupling to the adsorbed region.

Although both attachment scenarios S1 and S2 appear to some extent plausible, at present it is difficult to make reliable statements about their respective likelihood. In fact only a posteriori we can cautiously state that based on the experimental static and dynamic measurement ev-

idence: the chain "wobbles" to a high enough extent to display the effects that we observe.

-
- * Electronic address: [Email:]kulic@unistra.fr
- [1] Mohrbach, H., A. Johner, and I. M. Kulic. 2010. Tubulin bistability and polymorphic dynamics of microtubules. *Phys. Rev. Lett.* 105:268102.
 - [2] Howard, J., *Mechanics of Motor Proteins and the Cytoskeleton*, Sinauer Press 2001.
 - [3] Amos, L. A., and Amos W. G., *Molecules of the Cytoskeleton*, Guilford Press 1991.
 - [4] Kulic, I. M., A. E. X. Brown, H. Kim, C. Kural, B. Blehm, P. R. Selvin. 2008. The role of microtubule movement in bidirectional organelle transport. *Proc. Natl. Acad. Sci. USA.* 105:10011-10016.
 - [5] Alberts, B., A. Johnson, J. Lewis, M. Raff, K. Roberts, and P. Walter. 2005. *Molecular Biology of the Cell*.
 - [6] Nogales, E., M. Whittaker, R. A. Milligan, K. H. Downing 1999. High resolution model of the microtubule. *Cell.* 96:79-88.
 - [7] Huilin, J., D. J. DeRosier, W. V. Nicholson, E. Nogales, K. H. Downing. 2002. Microtubule Structure at 8 Å Resolution. *Structure.* 10:1317-1328.
 - [8] Nogales, E., S. G. Wolf, and K. H. Downing. 1998. Structure of the $\alpha\beta$ tubulin dimer by electron crystallography. *Nature.* 391:199-203.
 - [9] Löwel, J., H. Li, K. H. Downing and E. Nogales. 2001. Refined Structure of $\alpha\beta$ -Tubulin at 3.5 Å Resolution. *J. Mol. Biol.* 313:10451-057.
 - [10] Bouchet-Marquis, C., B. Zuber, A-M. Glynn, M. Eltsov, M. Grabenbauer, K. N. Goldie, D. Thomas, A. S. Frangakis, J. Dubochet, and D. Chrétien. 2007. Visualization of cell microtubules in their native state. *Bio. Cell.* 99:45-53.
 - [11] Wade, R. H., D. Chrétien, and D. Job. 1990. Characterization of microtubule protofilament numbers. How does the surface lattice accommodate?. *J. Mol. Bio.* 212:775-786.
 - [12] Chretien, D., and R. H. Wade. 1991. New data on the microtubule surface lattice. *Bio. Cell.* 71:161-174.
 - [13] Ray, S., E. Meyhofer, R. A. Milligan, and J. Howard. 1993. Kinesin follows the microtubule's protofilament axis. *J. Cell Biol.* 121:1083-1093.
 - [14] Chrétien, D., F. Metoz, F. Verde, E. Karsenti, and R. H. Wade. 1992. Lattice defects in microtubules: protofilament numbers vary within individual microtubules. *J. Cell. Biol.* 117:1031-1040.
 - [15] Chretien, D., and S. D. Fuller. 2000. Microtubules switch occasionally into unfavorable configurations during elongation. *J. Mol. Biol.* 298:663-676.
 - [16] Hunyadi, V., I. M. Janosi. 2007. Metastability of Microtubules Induced by Competing Internal Forces. *Biophys. J.* 92:3092-3097
 - [17] Mandelkow, E. M., E. Mandelkow, R. A. Milligan. 1991. Microtubules dynamics and microtubules caps: a time-resolved cryoelectron microscopy study. *J. Cell. Biol.* 114:977-991.
 - [18] Nogales, E., H. W. Wang, H. Niederstrasser. 2003. Tubulin rings: which way do they curve ?. *Curr. Opin. Struct. Biol.* 13:256-261.
 - [19] Mitchison, T., and M. W. Kirschner. 1984. Dynamic instability of microtubule growth. *Nature.* 312:237-242.
 - [20] Erickson, H. P., and E. T. O'Brien. 1992. Microtubule dynamic instability and GTP hydrolysis. *Annu. Rev. Biophys. Biomol. Struct.* 21:145-166.
 - [21] Janosi, I. M., Chretien, D. and Flyvbjerg, H. 2002. Structural microtubule cap: stability, catastrophe, rescue, and third state. *Biophys. J.* 83:1317-1330.
 - [22] Arnal, I., and R. H. Wade. 1995. How does taxol stabilize microtubules ?. *Curr. Biol.* 5:900-908.
 - [23] Amos, L. A., and J. Löwe. 1999. How taxol stabilises microtubule structure. *Chem. Biol.* 6:R65-R69.
 - [24] Xiao, H., P. Verdier-Pinard, N. Fernandez-Fuentes, B. Burd, R. Angeletti, A. Fiser, S. B. Horwitz, G. A. Orr. 2006. Insights into the mechanism of microtubule stabilization by taxol. *Proc. Natl. Acad. Sci. USA.* 103:10166-10173.
 - [25] Elie-Caille, C., F. Severin, J. Helenius, J. Howard, D. J. Muller, A. A. Hyman. 2007. Straight GDP-tubulin protofilaments form in the presence of taxol. *Curr. Biol.* 17:1765-1770.
 - [26] Gittes, F., B. Mickey, J. Nettleton, and J. Howard. 1993. Flexural rigidity of microtubules and actin filaments measured from thermal fluctuations in shape. *J. Cell Biol.* 120:923-934.
 - [27] Venier, P., A. C. Maggs, M. F. Carlier, and D. Pantaloni. 1994. Analysis of microtubule rigidity using hydrodynamic flow and thermal fluctuations. *J. Biol. Chem.* 269:13353
 - [28] Mickey, B., and J. Howard. 1995. Rigidity of microtubules is increased by stabilizing agents. *J. Cell Biol.* 130:909-917.
 - [29] Felgner, H., R. Frank, and M. Schliwa. 1996. Flexural rigidity of microtubules measured with the use of optical tweezers. *J. Cell Sci.* 109:509-516.
 - [30] Kikumoto, M., M. Kurachi, V. Tosa, and H. Tashiro. 2006. Flexural rigidity of individual microtubules measured by a buckling force with optical traps. *Biophys. J.* 90:1687-1696.
 - [31] Kurachi, M., M. Hoshi, and H. Tashiro. 1995. Buckling of a single microtubule by optical trapping forces: direct measurement of microtubule rigidity. *Cell Motil. Cytoskeleton.* 30:221-228.
 - [32] Takasone, T., S. Juodkazis, Y. Kawagishi, A. Yamaguchi, S. Matsuo, H. Sakakibara, H. Nakayama, and H. Misawa. 2002. Flexural rigidity of a single microtubule. *Jpn. J. Appl. Phys.* 41:3015-3019.
 - [33] Kis, A., S. Kasas, B. Babic, A. J. Kulik, W. Benoit, G. A. Briggs, C. Schonberger, S. Catsicas, and L. Forro. 2002. Nanomechanics of microtubules. *Phys. Rev. Lett.* 89:248101.
 - [34] Van den Heuvel, M. G. L., S. Bolhuis, and C. Dekker. 2007. Persistence length measurements from stochastic single-microtubule trajectories, *Nano Lett.* 7:3138.
 - [35] Van den Heuvel, M. G. L., M. P. de Graaff, and C. Dekker. 2008. Microtubule curvatures under perpendicular electric forces reveal a low persistence length. *Proc. Natl. Acad. Sci. USA* 105:7941.
 - [36] Kim, T., M. T. Kao, E. F. Hasselbrink, and E. Meyhöfer. 2008. Nanomechanical model of microtubule translocation in the presence of electric fields. *Biophys. J.* 94:3880-3892.
 - [37] Pampaloni, F., G. Lattanzi, A. Jonas, T. Surrey, E. Frey, and E. L. Florin. 2006. Thermal fluctuations of grafted

- microtubules provide evidence of a length-dependent persistence length. *Proc. Natl. Acad. USA*. 103:10248-10253.
- [38] Taute, K. M., F. Pampaloni, E. Frey, and E-L. Florin, 2008. Microtubule dynamics depart from the wormlike chain model. *Phys. Rev. Lett.* 100, 028102.
- [39] Brangwynne, C., G. Koenderink, E. Barry, Z. Dogic, F. MacKintosh, and D. Weitz. 2007. Bending dynamics of fluctuating biopolymers probed by automated high-resolution filament tracking. *Biophys. J.* 93:346-359.
- [40] Janson, M. E. and M. Dogterom. 2004. A bending mode analysis for growing microtubules: evidence for a velocity-dependent rigidity. *Biophys. J.* 87:2723-2736.
- [41] Van den Heuvel, M. G. L., M. P. de Graaff, S. G. Lemay, and C. Dekker. 2007. Electrophoresis of individual microtubules in microchannels. *Proc Natl Acad Sci U S A*. 104:7770-7775.
- [42] Amos, L. A., and W. B. Amos. 1991. The bending of sliding microtubules imaged by confocal light microscopy and negative stain electron microscopy. *J. Cell. Sci. Suppl.* 14:95-101.
- [43] Vale, R.D., C. M. Coppin, F. Malik, F. J. Kull, and R. D. Milligan. 1994. Tubulin GTP hydrolysis influences the structure, mechanical properties and kinesin-driven transport of microtubules. *J. Biol. Chem.* 269:23769-23775
- [44] Amos, L. A. Negative Stain electron microscopy of microtubules and associated motor molecules. 1991. *Micron and Microscopica Acta*. 22:395.
- [45] Heussinger, C., M. Bathe, and E. Frey. 2007. Statistical mechanics of semiflexible bundles of wormlike polymer chains. *Phys. Rev. Lett.* 99:048101.
- [46] Mohrbach, H., and I.M. Kulic. 2007. Motor driven microtubule shape fluctuations: force from within the lattice. *Phys. Rev. Lett.* 99:218102.
- [47] Chrétien, D., H. Flyvbjerg, and S. D. Fuller. 1998. Limited flexibility of the inter-protofilament bonds in microtubules assembled from pure tubulin. *Eur Biophys J* 27:490-500.
- [48] Bicek, A. D., E. Tüzel, A. Demtchouk, M. Uppalapati, W. O. Hancock, D. M. Kroll, and D. J. Odde. 2009. Anterograde microtubule transport drives microtubule bending in LLC-PK1 epithelial cells. *Molecular Biology of the Cell*. 20:2943.
- [49] Brangwynne, C. P., F. C. MacKintosh, S. Kumar, N. A. Geisse, J. Talbot, L. Mahadevan, K. K. Parker, D. E. Ingber, and D. A. Weitz. 2006. Microtubules can bear enhanced compressive loads in living cells because of lateral reinforcement. *J. Cell. Bio.* 173:733-741.
- [50] Keating T. J., J. G. Peloquin, V. I. Rodionov, D. Momcilovic, and G.G. Borisy. 1997. Microtubule release from the centrosome, *Proc. Natl. Acad. Sci. USA*. 94:5078.
- [51] Kaech, S., B. Ludin and A. Matus. 1996. Cytoskeletal Plasticity in Cells Expressing Neuronal Microtubule-Associated Proteins. *Neuron*. 17:1189
- [52] Samsonov A., J-Z. Yu, M. Rasenick and S. V. Popov. 2004. Tau interaction with microtubules in vivo. *J. Cell. Sci.* 117:6129.
- [53] Keller, P. J., F. Pampaloni, G. Lattanzi, and E. H. K. Stelzer. 2008. Three-dimensional microtubule behavior in *Xenopus* egg extracts reveals four dynamic states and state-dependent elastic properties. *Biophys. J.* 95:1474.
- [54] Fridoon, J. A., J. Hughey, T. Wittmann, A. Hyman, M. Greaser and P. W. Baas. 2000. Motor proteins regulate force interactions between microtubules and microfilaments in the axon. *Nature Cell Biol* 2:276.
- [55] Asakura, S. 1970. Polymerization of flagellin and polymorphism of flagella. *Adv. Biophys. (Japan)*. 1:99-155.
- [56] Calladine, C. R. 1975. Construction of bacterial flagella. *Nature (London)* 255:121-124.
- [57] Kol, N., L. Adler-Abramovich, D. Barlam, R. Z. Shneck, E. Gazit, and I. Rouso. 2005. Self-assembled peptide nanotubes are uniquely rigid bioinspired supramolecular structures. *Nano Lett.* 5:1343.
- [58] Desai, A., S. Verma, T. J. Mitchison and C. E. Walczak. 1999. Kin I kinesins are microtubule-destabilizing enzymes. *Cell* 96:69-78.
- [59] Hartman, J. J., J. Mahr, K. McNally, K. Okawa, A. Iwamatsu, S. Thomas, S. Cheesman, J. Heuser, R. D. Vale, and F. J. McNally. 1998. Katanin, a Microtubule-Severing Protein Is a Novel AAA ATPase that Targets to the Centrosome Using a WD40-Containing Subunit, *Cell* 93:277-287.
- [60] Davis, L. J., D. J. Odde, S. M. Block, and S. P. Gross. 2002. The Importance of Lattice Defects in Katanin-Mediated Microtubule Severing in Vitro. *Biophys. J.* 82:2916.
- [61] E. Muto, H. Sakai and K. Kaseda. 2005. Long-range cooperative binding of kinesin to a microtubule in the presence of ATP. *J. Cell Biol.* 168:691.
- [62] In Appendix E we discuss possible effects induced by surface attachment that could to some extent interfere with the ideal free "wobbling" motion in experiments.